
Robust Implicit Backpropagation

Francois Fagan
Columbia University
New York, NY, 10027
ff2316@columbia.edu

Garud Iyengar
Columbia University
New York, NY, 10027
garud@ieor.columbia.edu

Abstract

Arguably the biggest challenge in applying neural networks is tuning the hyper-parameters, in particular the learning rate. The sensitivity to the learning rate is due to the reliance on backpropagation to train the network. In this paper we present the first application of Implicit Stochastic Gradient Descent (ISGD) to train neural networks, a method known in convex optimization to be *unconditionally stable* and *robust to the learning rate*. Our key contribution is a novel layer-wise approximation of ISGD which makes its updates tractable for neural networks. Experiments show that our method is more robust to high learning rates and generally outperforms standard backpropagation on a variety of tasks.

1 Introduction

Despite decades of research, most neural networks are still optimized using minor variations on the backpropagation method proposed by Rumelhart, Hinton and Williams in 1986 [23]. Since backpropagation is a stochastic first order method, its run time per iteration is independent of the number of training datapoints. It is this key property that makes it able to ingest the vast quantities of data required to train neural networks on complex tasks like speech and image recognition.

A serious limitation of backpropagation being a first order method is its inability to use higher order information. This leads to multiple problems: the need to visit similar datapoints multiple times in order to converge to a good solution, instability due to “exploding” gradients [21, Sec. 3], and high sensitivity to the learning rate [10, Sec. 11.4.1]. A number of different approaches have been suggested to deal with these problems. Adaptive learning rate methods, like Adam [13] and Adagrad [7], estimate appropriate per-parameter learning rates; and momentum accelerates backpropagation in a common direction of descent [32]. Gradient clipping is a heuristic which “clips” the gradient magnitude at a pre-specified threshold and has been shown to help deal with exploding gradients [21, Sec. 3]. Although these approaches partially address the problems of backpropagation, neural network training remains unstable and highly sensitive to the learning rate [10, Sec. 11].

The key research question here is how to add higher order information to stabilize backpropagation while keeping the per iteration run time independent of the number of datapoints. A technique that has recently emerged that addresses this same question in the context of convex optimization is Implicit Stochastic Gradient Descent (ISGD). ISGD is known in convex optimization to be *robust to the learning rate* and *unconditionally stable* for convex optimization problems [24, Sec. 5][27, Sec. 3.1]. A natural question is whether ISGD can be used to improve the stability of neural network optimization.

In this paper, we show how ISGD can be applied to neural network training. To the best of our knowledge this is the first time ISGD has been applied to this problem.¹ The main challenge in applying ISGD is solving its implicit update equations. This step is difficult even for most convex

¹[28] recently remarked that ISGD hasn’t yet been applied to neural networks and is an open research question.

optimization problems. We leverage the special structure of neural networks by constructing a novel layer-wise approximation for the ISGD updates. The resulting algorithm, *Implicit Backpropagation* (IB), is a good trade-off: it has almost the same run time as the standard “Explicit” Backpropagation (EB), and yet enjoys many of the desirable features of exact ISGD. IB is compatible with many activation functions such as the relu, arctan, hardtanh and smoothstep; however, in its present form, it cannot be applied to convolutional layers. It is possible to use IB for some layers and EB for the other layers; thus, IB is partially applicable to virtually all neural network architectures.

Our numerical experiments demonstrate that IB is stable for much higher learning rates as compared to EB on classification, autoencoder and music prediction tasks. In all of these examples the learning rate at which IB begins to diverge is 20%-200% higher than for EB. We note that for small-scale classification tasks EB and IB have similar performance. IB performs particularly well for RNNs, where exploding gradients are most troublesome. We also investigate IB’s compatibility with clipping. We find that IB outperforms EB with clipping on RNNs, where clipping is most commonly used, and that clipping benefits both IB and EB for classification and autoencoding tasks. Overall, IB is clearly beneficial for RNN training and shows promise for classification and autoencoder feedforward neural networks. We believe that more refined implementations of ISGD to neural networks than IB are likely to lead to even better results — a topic for future research.

The rest of this paper is structured as follows. Section 2 reviews the literature on ISGD and related methods. Section 3 develops IB as approximate ISGD, with Section 4 deriving IB updates for multiple activation functions. The empirical performance of IB is investigated in Section 5 and we conclude with mentions of further work in Section 6.

2 ISGD and related methods

2.1 ISGD method

The standard objective in most machine learning models, including neural networks, is the ridge-regularized loss

$$\ell(\theta) = \frac{1}{N} \sum_{i=1}^N \ell_i(\theta) + \frac{\mu}{2} \|\theta\|_2^2,$$

where $\ell_i(\theta) = \ell_\theta(x_i, y_i)$ is the loss associated with i^{th} datapoint (x_i, y_i) and θ comprises the weight and bias parameters in the neural network.

The method ISGD uses to minimize $\ell(\theta)$ is similar to that of standard “Explicit” SGD (ESGD). In each iteration of ESGD, we first sample a random datapoint i and then update the parameters as $\theta^{(t+1)} = \theta^{(t)} - \eta_t(\nabla_{\theta} \ell_i(\theta^{(t)}) + \mu\theta^{(t)})$, where η_t is the learning rate at time t . ISGD also samples a random datapoint i but employs the update $\theta^{(t+1)} = \theta^{(t)} - \eta_t(\nabla_{\theta} \ell_i(\theta^{(t+1)}) + \mu\theta^{(t+1)})$, or equivalently,

$$\theta^{(t+1)} = \arg \min_{\theta} \left\{ 2\eta_t(\ell_i(\theta) + \frac{\mu}{2} \|\theta\|_2^2) + \|\theta - \theta^{(t)}\|_2^2 \right\}. \quad (1)$$

The main motivation of ISGD over ESGD is its *robustness to learning rates*, *numerical stability* and *transient convergence behavior* [2, 22, 24]. The increased robustness of ISGD over ESGD can be illustrated with a simple quadratic loss $\ell(\theta) = \frac{1}{2} \|\theta\|_2^2$, as displayed in Figure 1. Here the ISGD step $\theta^{(t+1)} = \theta^{(t)} / (1 + \eta_t)$ is stable for any learning rate whereas the ESGD step $\theta^{(t+1)} = \theta^{(t)}(1 - \eta_t)$ diverges when $\eta_t > 2$.

Since ISGD becomes equivalent to ESGD when the learning rate is small, there is no difference in their asymptotic convergence rate for decreasing learning rates. However, it is often the case that in the initial iterations, when the learning rate is still large, ISGD outperforms ESGD.

The main drawback of ISGD is that the implicit update (1) can be expensive to compute, whereas the update for ESGD is usually trivial. If this update is expensive, then ESGD may converge faster than ISGD in terms of wall clock time, even if ISGD converges faster per epoch. Thus, in order for ISGD to be effective, one needs to be able to solve the update (1) efficiently. Indeed, the focus of this paper is to develop a methodology for efficiently approximating the ISGD update for neural networks.

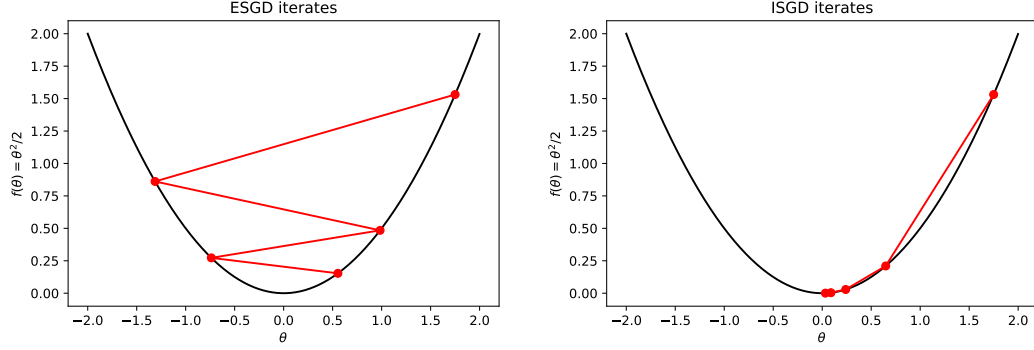


Figure 1: Illustration of the difference between ESGD and ISGD in optimizing $f(\theta) = \theta^2/2$. The learning rate is $\eta = 1.75$ in both cases.

2.2 Related methods

ISGD has been successfully applied to several machine learning tasks. Cheng et al. [5] applied ISGD to learning online kernels and He [11] to SVMs, while Kulis and Bartlett [15] consider a range of problems including online metric learning. ISGD has also been used to improve the stability of temporal difference algorithms in reinforcement learning [12, 26]. For more recent advances in ISGD see [3, 17, 20, 29, 30].

Although ISGD has never been applied to neural networks, closely related methods have been investigated. ISGD may be viewed as a trust-region method, where $1/2\eta$ is the optimal dual variable in the Lagrangian,

$$\arg \min_{\theta} \left\{ \ell_i(\theta) + \frac{\mu}{2} \|\theta\|_2^2 : \|\theta - \theta^{(t)}\|_2^2 \leq r \right\} = \arg \min_{\theta} \left\{ \ell_i(\theta) + \frac{\mu}{2} \|\theta\|_2^2 + \frac{1}{2\eta(r)} \|\theta - \theta^{(t)}\|_2^2 \right\}.$$

Trust-region methods for optimizing neural networks have been effectively used to stabilize policy optimization in reinforcement learning [25, 31]. Clipping, which truncates the gradient at a pre-specified threshold, may also be viewed as a computationally efficient approximate trust-region method [21]. It was explicitly designed to address the exploding gradient problem and achieves this by truncating the exploded step. In the experiments section we will investigate the difference in the effect of IB and clipping.

An example of a non-trust region method for optimizing neural networks using higher order information is Hessian-Free optimization [18, 19]. These methods directly estimate second order information of a neural network. They have been shown to make training more stable and require fewer epochs for convergence. However they come at a much higher per iteration cost than first order methods, which offsets this benefit [1].

3 Implicit Backpropagation

In this section we develop Implicit Backpropagation (IB) as an approximate ISGD implementation for neural networks. It retains many of the desirable characteristics of ISGD, while being virtually as fast as the standard ‘‘Explicit’’ Backpropagation (EB).

Consider a d -layered neural network $f_{\theta}(x) = f_{\theta_d}^{(d)} \circ f_{\theta_{d-1}}^{(d-1)} \circ \dots \circ f_{\theta_1}^{(1)}(x)$ where $f_{\theta_k}^{(k)} : \mathbb{R}^{D_k} \rightarrow \mathbb{R}^{D_{k+1}}$ represents the k^{th} layer with parameters $\theta_k \in \mathbb{R}^{P_k}$, $\theta = (\theta_1, \dots, \theta_d)$, $x \in \mathbb{R}^{D_1}$ is the input to the neural network, and \circ denotes composition. Let the loss associated with a datapoint (x, y) be $\ell_{\theta}(x, y) = \ell(y, \cdot) \circ f_{\theta}(x)$ for some $\ell(y, \cdot) : \mathbb{R}^{D_{d+1}} \rightarrow \mathbb{R}$. Later in this section, we will want to extract the effect of the k^{th} layer on the loss. To this end, we can rewrite the loss as $\ell_{\theta}(x, y) = \ell_{\theta_{d:k+1}, y}^{(d:k+1)} \circ f_{\theta_k}^{(k)} \circ f_{\theta_{k-1:1}}^{(k-1:1)}(x)$ where $f_{\theta_{i:j}}^{(i:j)} = f_{\theta_i}^{(i)} \circ f_{\theta_{i-1}}^{(i-1)} \circ \dots \circ f_{\theta_j}^{(j)} : \mathbb{R}^{D_i} \rightarrow \mathbb{R}^{D_{j+1}}$ and $\ell_{\theta_{a:j}}^{(d:j)} = \ell(y, \cdot) \circ f_{\theta_{a:j}}^{(d:j)} : \mathbb{R}^{D_j} \rightarrow \mathbb{R}$.

The complexity of computing the ISGD update depends on the functional form of the loss $\ell_\theta(x, y)$. Although it is possible in some cases to compute the ISGD update explicitly, this is not the case for neural networks. Even computing the solution numerically is very expensive. Hence, it is necessary to approximate the ISGD update in order for it to be computationally tractable. We introduce the following two approximations in IB:

- (a) We update parameters layer by layer. When updating parameter θ_k associated with layer k , all the parameters $\theta_{-k} = \{\theta_i : i \neq k\}$ corresponding to the other layers are kept fixed. Under this approximation the loss when updating the k^{th} layer is

$$\ell_k(\theta_k; x, y, \theta_{-k}^{(t)}) := \ell_{\theta_{d:k+1,y}^{(d:k+1)}}^{(d:k+1)} \circ f_{\theta_k}^{(k)} \circ f_{\theta_{k-1:1}^{(k-1:1)}}^{(k-1:1)}(x). \quad (2)$$

- (b) Building on (a), we linearize the higher layers $\ell_{\theta_{d:k+1,y}^{(d:k+1)}}^{(d:k+1)}$, but keep the layer being updated $f_{\theta_k}^{(k)}$ as non-linear. The loss from (2) reduces to²

$$\tilde{\ell}_k(\theta_k; x, y, \theta_{-k}^{(t)}) := \ell_{\theta_{d:k+1,y}^{(d:k+1)}}(x, y) + \nabla \ell_{\theta_{d:k+1,y}^{(d:k+1)}}^{(d:k+1)\top} (f_{\theta_k}^{(k)} \circ f_{\theta_{k-1:1}^{(k-1:1)}}^{(k-1:1)}(x) - f_{\theta_{k:1}^{(k:1)}}^{(k:1)}(x)). \quad (3)$$

This approximation can be validated via a Taylor series expansion where the error in (3) compared to (2) is $O(\|\theta_k - \theta_k^{(t)}\|_2^2)$.

The IB approximation to the ISGD update is, thus, given by

$$\theta_k^{(t+1)} = \arg \min_{\theta_k} \left\{ 2\eta \left(\tilde{\ell}_k(\theta_k; x, y, \theta_{-k}^{(t)}) + \frac{\mu}{2} \|\theta_k\|_2^2 \right) + \|\theta_k - \theta_k^{(t)}\|_2^2 \right\}. \quad (4)$$

In Appendix C we present a simple theorem, which leverages the fact that IB converges to EB in the limit of small learning rates, to show that IB converges to a stationary point of $\ell(\theta)$ for appropriately decaying learning rates.

In the next section we show that the IB update can be efficiently computed for a variety of activation functions. The IB approximations thus make ISGD practically feasible to implement. However, the approximation is not without drawbacks. The layer-by-layer update from (a) removes all higher order information along directions perpendicular to the parameter space of the layer being updated, and the linearization in (b) loses information about the non-linearity in the higher layers. The hope is that IB retains enough of the beneficial properties of ISGD to have noticeable benefits over EB. In our experiments we show that this is indeed the case.

Our IB formulation is, to our knowledge, novel. The most similar update in the literature is for composite convex optimization with just two layers, where the lower, not higher, layer is linearized [8].

4 Implicit Backpropagation updates for various activation functions

Since neural networks are applied to extremely large datasets, it is important that the IB updates can be computed efficiently. In this section we show that the IB update (4) can be greatly simplified, resulting in fast analytical updates for activation functions such as the relu and arctan. For those activation functions that do not have an analytical IB update, IB can easily be applied on a piecewise-cubic approximation of the activation function. This makes IB practically applicable to virtually any element-wise acting activation function.

Although it is possible to apply IB to layers with weight sharing or non-element-wise acting activation functions, the updates tend to be complex and expensive to compute. For example, the IB update for a convolutional layer with max-pooling and a relu activation function involves solving a quadratic program with binary variables (see Appendix B for the derivation). Thus, we will only focus on updates for activation functions that are applied element-wise and have no shared weights.

²Note that the derivative $\nabla_{\theta_{d:k+1,y}^{(d:k+1)}} \ell_{\theta_{d:k+1,y}^{(d:k+1)}}^{(d:k+1)}$ is taken with respect to its argument $f_{\theta_{k:1}^{(k:1)}}^{(k:1)}(x) \in \mathbb{R}^{D^{k+1}}$, not $\theta_{d:k+1}$.

4.1 Generic updates

Here we derive the IB updates for a generic layer k with element-wise acting activation function σ . Let the parameters in the k^{th} layer be $\theta_k = (W_k, B_k) \in \mathbb{R}^{D_{k+1} \times (1+D_k)}$ where $W_k \in \mathbb{R}^{D_{k+1} \times D_k}$ is the weight matrix and $B_k \in \mathbb{R}^{D_{k+1}}$ is the bias. We'll use the shorthand notation $z^{ki} = (f_{\theta_{k-1:1}}^{(k-1:1)}(x_i), 1) \in \mathbb{R}^{1+D_k}$ for the input to the k^{th} layer and $b^{ki} = \nabla_{\theta_{d:k+1,y}^{(t)}} \ell_{\theta^{(t)}}^{(d:k+1)} \in \mathbb{R}^{D_{k+1}}$

for the backpropagated gradient. The output of the k^{th} layer is thus $\sigma(\theta_k z^{ki})$ where σ is applied element-wise and $\theta_k z^{ki}$ is a matrix-vector product. Using this notation the IB update from (4) becomes:

$$\theta_k^{(t+1)} = \arg \min_{\theta_k} \left\{ 2\eta_t b^{ki\top} \sigma(\theta_k z^{ki}) + \eta_t \mu \|\theta_k\|_2^2 + \|\theta_k - \theta_k^{(t)}\|_2^2 \right\}, \quad (5)$$

where we have dropped the terms $\ell_{\theta^{(t)}}(x, y)$ and $b^{ki\top} f_{\theta_{k:1}^{(k:1)}}^{(k:1)}(x)$ from (3) as they are constant with respect to θ_k . Now that we have written the IB update in more convenient notation, we can begin to simplify it. Due to the fact that σ is applied element-wise, (5) breaks up into D_{k+1} separate optimization problems, one for each output node $j \in \{1, \dots, D_{k+1}\}$:

$$\theta_{kj}^{(t+1)} = \arg \min_{\theta_{kj}} \left\{ 2\eta_t b_j^{ki} \sigma(\theta_{kj}^\top z^{ki}) + \eta_t \mu \|\theta_{kj}\|_2^2 + \|\theta_{kj} - \theta_{kj}^{(t)}\|_2^2 \right\}, \quad (6)$$

where $\theta_{kj} = (W_{kj}, B_{kj}) \in \mathbb{R}^{1+D_k}$ are the parameters corresponding to the j^{th} output node. Using simple calculus we can write the solution to $\theta_{kj}^{(t+1)}$ as

$$\theta_{kj}^{(t+1)} = \frac{\theta_{kj}^{(t)}}{1 + \eta_t \mu} - \eta_t \alpha_j^{ki} z^{ki} \quad (7)$$

where $\alpha_j^{ki} \in \mathbb{R}$ is the solution to the one-dimensional optimization problem

$$\alpha_j^{ki} = \arg \min_{\alpha} \left\{ b_j^{ki} \cdot \sigma \left(\frac{\theta_{kj}^{(t)\top} z^{ki}}{1 + \eta_t \mu} - \alpha \cdot \eta_t \|z^{ki}\|_2^2 \right) + \eta_t (1 + \eta_t \mu) \|z^{ki}\|_2^2 \frac{\alpha^2}{2} \right\}. \quad (8)$$

See Appendix A for the derivation.

To connect the IB update to EB, observe that if we do a first order Taylor expansion of (7) and (8) in η_t we recover the EB update:

$$\theta_{kj}^{(t+1)} = \theta_{kj}^{(t)} (1 - \eta_t \mu) - \eta_t \sigma' \left(\theta_{kj}^{(t)\top} z^{ki} \right) b_j^{ki} z^{ki} + O(\eta_t^2),$$

where σ' denotes the derivative of σ . Thus we can think of IB as a higher order update than EB.

In summary, the original $D_{k+1} \times D_k$ dimensional IB update from (5) has been reduced to D_{k+1} separate one-dimensional optimization problems in the form of (8). The difficulty of solving (8) depends on the activation function σ . Since (8) is a one-dimensional problem, an optimal α can always be computed numerically using the bisection method, although this may be slow. Fortunately there are certain important activation functions for which α can be computed analytically. In the subsections below we derive analytical updates for α when σ is the relu and arctan functions as well as a general formula for piecewise-cubic functions.

Before proceeding to these updates, we can observe directly from (7) and (8) that IB will be robust to high learning rates. Unlike EB, in which the step size increases linearly with the learning rate, IB has a bounded step size even for infinite learning rates. As the learning rate increases (7) becomes

$$\theta_{kj}^{(t+1)} \xrightarrow{\eta_t \rightarrow \infty} \arg \min_{\beta} \left\{ b_j^{ki} \cdot \sigma \left(\beta \cdot \|z^{ki}\|_2^2 \right) + \mu \|z^{ki}\|_2^2 \frac{\beta^2}{2} \right\} z^{ki}$$

where $\beta = -\eta_t \alpha$. This update is finite as long as $\mu > 0$ and σ is asymptotically linear.

4.2 Relu update

Here we give the solution to α from (8) for the relu activation function, $\sigma(x) = \max\{x, 0\}$. We will drop the super- and sub-scripts from (8) for notational convenience. When $\text{sign}(b) = +1$ there are

Table 1: IB relu updates

$Sign(b) = +1$	$Sign(b) = -1$
$\alpha = \begin{cases} 0 & \text{if } \theta^\top z \leq 0 \\ \frac{\theta^\top z}{1+\eta\mu} \frac{1}{\eta\ z\ _2^2} & \text{if } 0 < \theta^\top z \leq \eta\ z\ _2^2 b \\ \frac{b}{1+\eta\mu} & \text{if } \theta^\top z > \eta\ z\ _2^2 b \end{cases}$	$\alpha = \begin{cases} 0 & \text{if } \theta^\top z \leq \frac{1}{2}\eta\ z\ _2^2 b \\ \frac{b}{1+\eta\mu} & \text{if } \theta^\top z > \frac{1}{2}\eta\ z\ _2^2 b \end{cases}$

three cases and when $sign(b) = +1$ there are two cases for the solution to α . The updates are given in Table 1.

The difference between the EB and IB updates is illustrated in Figure 2. When $sign(b) = +1$ and $\theta^\top z$ is on the slope but close to the hinge, the EB step overshoots the hinge point, making a far larger step than is necessary to reduce the relu to 0. IB, on the other hand, stops at the hinge. The IB update is better from two perspectives. First, it is able to improve the loss on the given datapoint just as much as EB, but without taking as large a step. Assuming that the current value of θ is close to a minimizer of the average loss of the other datapoints, an unnecessarily large step will likely take θ away its (locally) optimum value. An example of where this property might be particularly important is for the ‘‘cliff’’ of ‘‘exploding gradient’’ problem in RNNs [21]. And second, the IB step size is a continuous function of θ , unlike in EB where the step size has a discontinuity at the origin. This should make the IB update more robust to perturbations in the data.

When $sign(b) = -1$ and $\theta^\top z$ is on the flat, EB isn’t able to descend as the relu has ‘‘saturated’’ (i.e. is flat). IB, on the other hand, can look past the hinge and is still able to descend down the slope, thereby decreasing the loss. IB thus partially solves the saturating gradient problem [21].

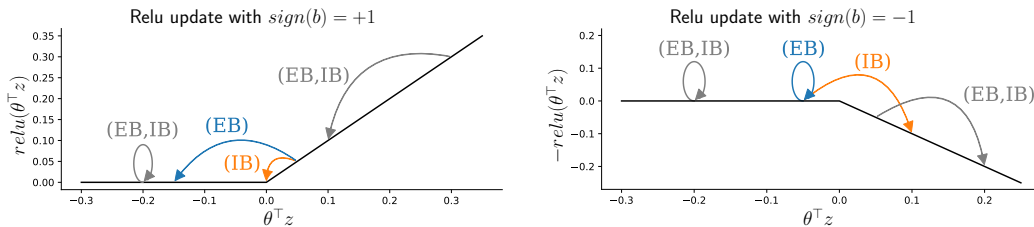
4.3 Arctan update

Although the IB update is not analytically available for all sigmoidal activation functions, it is available when σ is the arctan. For the arctan the value of α becomes the root of a cubic equation which can be solved for analytically. Since the arctan function is non-convex there may be up to three real solutions for α . Under the axiom that smaller step sizes that achieve the same decrease in the objective are better (as argued in Section 4.2), we always choose the value of α closest to zero.

4.4 Piecewise-cubic function update

Many activation functions are piecewise-cubic, including the hardtanh and smoothstep. Furthermore, all common activation functions can be approximated arbitrarily well with a piecewise-cubic. Being able to do IB updates for piecewise-cubic functions thus extends its applicability to virtually all activation functions.

Let $\sigma(x) = \sum_{m=1}^M I[B_m \leq x < B_{m+1}] \cdot \sigma_m(x)$ where $\sigma_m(x)$ is a cubic function and $B_m \in [-\infty, \infty]$ defines the bounds on each piece. The optimal value of α for each m can be found by evaluating σ_m at its boundaries and stationary points (which may be found by solving a quadratic equation). The value of α can then be solved for by iterating over $m = 1, \dots, M$ and taking the minimum over all the pieces. Since there are M pieces, the time to calculate α scales as $O(M)$.

Figure 2: Relu updates for EB and IB with $\mu = 0$. Lower values are better.

4.5 Relative run time difference of IB vs EB measured in flops

A crucial aspect of any neural network algorithm is not only its convergence rate per epoch, but also its run time. Since IB does extra calculations, it is slower than EB. Here we show that the difference in floating point operations (flops) between EB and IB is typically small, on the order of 30% or less.

For any given layer, let the input dimension be denoted as n and the output dimension as m . The run time of both EB and IB are dominated by three operations costing nm flops: multiplying the weight matrix and input in the forward propagation, multiplying the backpropagated gradient and input for the weight matrix gradient, and multiplying the backpropagated gradient and weight matrix for the backpropagated gradient in the lower layer. IB has two extra calculations as compared to EB: calculating $\|z^{ki}\|_2^2$, costing $2n$ flops, and calculating α_j^{ki} a total of m times, once for each output node. Denoting the number of flops to calculate each α_j^{ki} with activation function σ as c_σ , the relative increase in run time of IB over EB is upper bounded by $(2n + c_\sigma m)/(3nm)$.

The relative run time increase of IB over EB depends on the values of n , m and c_σ . When σ is the relu, then c_σ is small, no more than 10 flops; whereas when σ is the arctan c_σ is larger, costing just less than 100 flops.³ Taking these flop values as upper bounds, if $n = m = 100$ then the relative run time increase is upper bounded by 4% for relu and 34% for arctan. These bounds diminish as n and m grow. If $n = m = 1000$, then the bounds become just 0.4% for relu and 3.4% for arctan. Thus, IB's run time is virtually the same as EB's for large neural network tasks.

If n and m are small then the arctan IB update might be too slow relative to EB for the IB update to be worthwhile. In this case simpler sigmoidal activation functions, such as the hardtanh or smoothstep, may be preferable for IB. The hardtanh has been used before in neural networks, mainly in the context of binarized networks [6]. It has the form

$$\sigma(x) = \begin{cases} -1 & \text{if } x < -1 \\ x & \text{if } -1 \leq x \leq 1 \\ 1 & \text{if } x > 1 \end{cases}$$

for which c_σ is no more than 15 flops (using the piecewise-cubic function update from Section 4.4). The smoothstep is like the hardtanh but is both continuous and has continuous first derivatives,

$$\sigma(x) = \begin{cases} -1 & \text{if } x < -1 \\ \frac{3}{2}x - \frac{1}{2}x^3 & \text{if } -1 \leq x \leq 1 \\ 1 & \text{if } x > 1, \end{cases}$$

with c_σ being no more than 25 flops. The relative increase in run time of IB over EB for the hardtanh and smoothstep is about the same as for the relu. This makes the IB update with the hardtanh or smoothstep practical even if n and m are small.

5 Experiments

This section details the results of three sets of experiments where the robustness to the learning rate of IB is compared to that of EB.⁴ Since IB is equivalent to EB when the learning rate is small, we expect little difference between the methods in the limit of small learning rates. However, we expect that IB will be more stable and have lower loss than EB for larger learning rates.

Classification, autoencoding and music prediction tasks. For the first set of experiments, we applied IB and EB to three different but common machine learning tasks. The first task was image classification on the MNIST dataset [16] with an architecture consisting of two convolutional layers, an arctan layer and a relu layer. The second task also uses the MNIST dataset, but for an 8 layer relu autoencoding architecture. The third task involves music prediction on four music datasets, JSB Chorales, MuseData, Nottingham and Piano-midi.de [4], for which a simple RNN architecture is used with an arctan activation function.

For each dataset-architecture pair we investigated the performance of EB and IB over a range of learning rates where EB performs well (see Appendix D.5 for more details on how these learning rates

³The number of flops for arctan was counted using Cardano's method for optimizing the cubic equation.

⁴A more extensive description of the experimental setup and results are given in Appendices D and E.

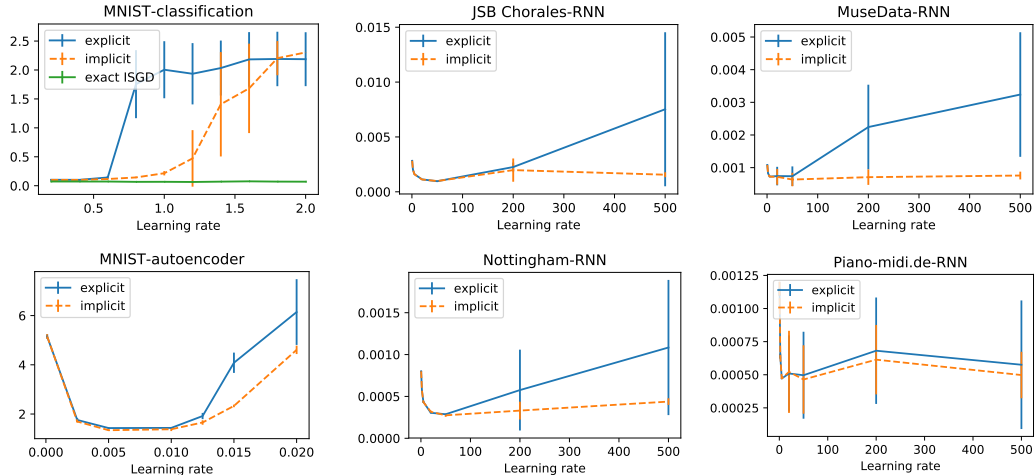


Figure 3: Training loss of EB and IB (lower is better). The plots display the mean performance and one standard deviation errors. The MNIST-classification plot also shows an “exact” version of ISGD with an inner gradient descent optimizer.

were chosen). Since IB and EB have similar asymptotic convergence rates, the difference between the methods will be most evident in the initial epochs of training. In our experiments we only focus on the performance after the first epoch of training for the MNIST datasets, and after the fifth epoch for the music datasets.⁵ Five random seeds are used for each configuration in order to understand the variance of the performance of the methods.⁶

Figure 3 displays the results for the experiments. EB and IB have near-identical performance when the learning rate is small. However, as the learning rate increases, the performance of EB deteriorates far more quickly as compared to IB. Over the six datasets, the learning rate at which IB starts to diverge is at least 20% higher than that of EB.⁷ The benefit of IB over EB is most noticeable for the music prediction problems where for high learning rates IB has much better mean performance and lower variance than EB. A potential explanation for this behaviour is that IB is better able to deal with exploding gradients, which are more prevalent in RNN training.

Exact ISGD. For MNIST-classification we also investigate the potential performance of *exact* ISGD. Instead of using our IB approximation for the ISGD update, we directly optimize (1) using gradient descent. For each ISGD update we take a total of 100 gradient descent steps of (1) at a learning rate 10 times smaller than the “outer” learning rate η_t . It is evident from Figure 3 that this method achieves the best performance and is remarkably robust to the learning rate. Since exact ISGD uses 100 extra gradient descent steps per iteration, it is 100 times slower than the other methods, and is thus impractically slow. However, its impressive performance indicates that ISGD-based methods have great potential for neural networks.

Run times. According to the bounds derived in Section 4.5, the run time of IB should be no more than 12% longer per epoch than EB on any of our experiments. With our basic Pytorch implementation IB took between 16% and 216% longer in practice, depending on the architecture used (see Appendix E.1 for more details). With a more careful implementation of IB we expect these run times to decrease to at least the levels indicated by the bounds. Using activation functions with more efficient IB updates, like the smoothstep instead of arctan, would further reduce the run time.

UCI datasets. Our second set of experiments is on 121 classification datasets from the UCI database [9]. We consider a 4 layer feedforward neural network run for 10 epochs on each dataset. In contrast

⁵The music datasets have fewer training examples and so more epochs are needed to see convergence.

⁶The same seeds are used for both EB and IB. Five seeds are used for all experiments, except MNIST-classification where twenty seeds are used.

⁷The threshold for divergence that we use is when the mean loss exceeds the average of EB’s minimum and maximum mean losses measured on that dataset over the various learning rates.

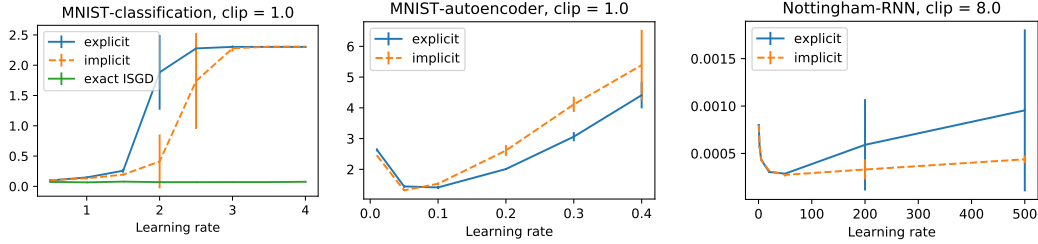


Figure 4: Training loss of EB with clipping and IB with clipping on three dataset-architecture pairs.

to the above experiments, we use the same coarse grid of 10 learning rates between 0.001 and 50 for all datasets. For each algorithm and dataset the best performing learning rate was found on the training set (measured by the performance on the training set). The neural network trained with this learning rate was then applied to the test set. Overall we found IB to have a 0.13% higher average accuracy on the test set. The similarity in performance of IB and EB is likely due to the small size of the datasets (some datasets have as few as 4 features) and relatively shallow architecture making the network relatively easy to train, as well as the coarseness of the learning rate grid.

Clipping. In our final set of experiments we investigated the effect of clipping on IB and EB. Both IB and clipping can be interpreted as approximate trust-region methods. Consequently, we expect IB to be less influenced by clipping than EB. This was indeed observed in our experiments. A total of 9 experiments were run with different clipping thresholds applied to RNNs on the music datasets (see Appendix D for details). Clipping improved EB’s performance for higher learning rates in 7 out of the 9 experiments, whereas IB’s performance was only improved in 2. IB without clipping had an equal or lower loss than EB with clipping for all learning rates in all experiments except for one (Piano-midi.de with a clipping threshold of 0.1). This suggests that IB is a more effective method for training RNNs than EB with clipping.

The effect of clipping on IB and EB applied to MNIST-classification and MNIST-autoencoder is more complicated. In both cases clipping enabled IB and EB to have lower losses for higher learning rates. For MNIST-classification it is still the case that IB has uniformly superior performance to EB, but for MNIST-autoencoder this is reversed. It is not unsurprising that EB with clipping may outperform IB with clipping. If the clipping threshold is small enough then the clipping induced trust region will be smaller than that induced by IB. This makes EB with clipping and IB with clipping act the same for large gradients; however, below the clipping threshold EB’s unclipped steps may be able to make more progress than IB’s dampened steps. See Figure 4 for plots of EB and IB’s performance with clipping.

Summary. We ran a total of 17 experiments on the MNIST and music datasets⁸. IB outperformed EB in 15 out of these. On the UCI datasets IB had slightly better performance than EB on average. The advantage of IB is most pronounced for RNNs, where for large learning rates IB has much lower losses and even consistently outperforms EB with clipping. Although IB takes slightly longer to train, this is offset by its ability to get good performance with higher learning rates, which should enable it to get away with less hyperparameter tuning.

6 Conclusion

In this paper we developed the first method for applying ISGD to neural networks. We showed that, through careful approximations, ISGD can be made to run nearly as quickly as standard backpropagation while still retaining the property of being more robust to high learning rates. The resulting method, which we call Implicit Backpropagation, consistently matches or outperforms standard backpropagation on image recognition, autoencoding and music prediction tasks; and is particularly effective for robust RNN training.

⁸MNIST-classification with and without clipping, MNIST-autoencoder with and without clipping, the four music datasets without clipping and nine experiments on the music datasets with clipping.

The success of IB demonstrates the potential of ISGD methods to improve neural network training. It may be the case that there are better ways to approximate ISGD than IB, which could produce even better results. For example, the techniques behind Hessian-Free methods could be used to make a quadratic approximation of the higher layers in IB (opposed to the linear approximation currently used); or a second order approximation could be made directly to the ISGD formulation in (1). Developing and testing such methods is a ripe area for future research.

References

- [1] Yoshua Bengio, Nicolas Boulanger-Lewandowski, and Razvan Pascanu. Advances in optimizing recurrent networks. In *Acoustics, Speech and Signal Processing (ICASSP), 2013 IEEE International Conference on*, pages 8624–8628. IEEE, 2013.
- [2] Dimitri P Bertsekas. Incremental proximal methods for large scale convex optimization. *Mathematical programming*, 129(2):163, 2011.
- [3] Dimitri P Bertsekas. Incremental aggregated proximal and augmented lagrangian algorithms. *arXiv preprint arXiv:1509.09257*, 2015.
- [4] Nicolas Boulanger-Lewandowski, Yoshua Bengio, and Pascal Vincent. Modeling temporal dependencies in high-dimensional sequences: Application to polyphonic music generation and transcription. *arXiv preprint arXiv:1206.6392*, 2012.
- [5] Li Cheng, Dale Schuurmans, Shaojun Wang, Terry Caelli, and Svn Vishwanathan. Implicit online learning with kernels. In *Advances in neural information processing systems*, pages 249–256, 2007.
- [6] Matthieu Courbariaux, Yoshua Bengio, and Jean-Pierre David. Binaryconnect: Training deep neural networks with binary weights during propagations. In *Advances in neural information processing systems*, pages 3123–3131, 2015.
- [7] John Duchi, Elad Hazan, and Yoram Singer. Adaptive subgradient methods for online learning and stochastic optimization. *Journal of Machine Learning Research*, 12(Jul):2121–2159, 2011.
- [8] John Duchi and Feng Ruan. Stochastic methods for composite optimization problems. *arXiv preprint arXiv:1703.08570*, 2017.
- [9] Manuel Fernández-Delgado, Eva Cernadas, Senén Barro, and Dinani Amorim. Do we need hundreds of classifiers to solve real world classification problems. *J. Mach. Learn. Res.*, 15(1):3133–3181, 2014.
- [10] Ian Goodfellow, Yoshua Bengio, and Aaron Courville. *Deep Learning*. MIT Press, 2016. <http://www.deeplearningbook.org>.
- [11] Kun He. *Stochastic functional descent for learning Support Vector Machines*. PhD thesis, 2014.
- [12] Ryo Iwaki and Minoru Asada. Implicit incremental natural actor critic. In *International Conference on Neural Information Processing*, pages 749–758. Springer, 2017.
- [13] Diederik P Kingma and Jimmy Ba. Adam: A method for stochastic optimization. *arXiv preprint arXiv:1412.6980*, 2014.
- [14] Günter Klambauer, Thomas Unterthiner, Andreas Mayr, and Sepp Hochreiter. Self-normalizing neural networks. In *Advances in Neural Information Processing Systems*, pages 972–981, 2017.
- [15] Brian Kulis and Peter L Bartlett. Implicit online learning. In *Proceedings of the 27th International Conference on Machine Learning (ICML-10)*, pages 575–582. Citeseer, 2010.
- [16] Yann LeCun. The mnist database of handwritten digits. <http://yann.lecun.com/exdb/mnist/>, 1998.
- [17] Hongzhou Lin, Julien Mairal, and Zaid Harchaoui. Catalyst acceleration for first-order convex optimization: from theory to practice. *arXiv preprint arXiv:1712.05654*, 2017.
- [18] James Martens. Deep learning via hessian-free optimization. In *ICML*, volume 27, pages 735–742, 2010.
- [19] James Martens and Ilya Sutskever. Learning recurrent neural networks with hessian-free optimization. In *Proceedings of the 28th International Conference on Machine Learning (ICML-11)*, pages 1033–1040. Citeseer, 2011.
- [20] Courtney Paquette, Hongzhou Lin, Dmitriy Drusvyatskiy, Julien Mairal, and Zaid Harchaoui. Catalyst acceleration for gradient-based non-convex optimization. *arXiv preprint arXiv:1703.10993*, 2017.
- [21] Razvan Pascanu, Tomas Mikolov, and Yoshua Bengio. On the difficulty of training recurrent neural networks. In *International Conference on Machine Learning*, pages 1310–1318, 2013.
- [22] Andrei Patrascu and Ion Necoara. Nonasymptotic convergence of stochastic proximal point algorithms for constrained convex optimization. *arXiv preprint arXiv:1706.06297*, 2017.

- [23] David E Rumelhart, Geoffrey E Hinton, and Ronald J Williams. Learning representations by back-propagating errors. *nature*, 323(6088):533, 1986.
- [24] Ernest K Ryu and Stephen Boyd. Stochastic proximal iteration: a non-asymptotic improvement upon stochastic gradient descent. *Author website, early draft*, 2014.
- [25] John Schulman, Sergey Levine, Pieter Abbeel, Michael Jordan, and Philipp Moritz. Trust region policy optimization. In *International Conference on Machine Learning*, pages 1889–1897, 2015.
- [26] Aviv Tamar, Panos Toulis, Shie Mannor, and Edoardo M Airoldi. Implicit temporal differences. *arXiv preprint arXiv:1412.6734*, 2014.
- [27] Panos Toulis and Edoardo M Airoldi. Scalable estimation strategies based on stochastic approximations: classical results and new insights. *Statistics and computing*, 25(4):781–795, 2015.
- [28] Panos Toulis, Thibaut Horel, and Edoardo M Airoldi. Stable robbins-monro approximations through stochastic proximal updates.
- [29] Panos Toulis, Dustin Tran, and Edo Airoldi. Towards stability and optimality in stochastic gradient descent. In *Artificial Intelligence and Statistics*, pages 1290–1298, 2016.
- [30] Jialei Wang, Weiran Wang, and Nathan Srebro. Memory and communication efficient distributed stochastic optimization with minibatch prox. *arXiv preprint arXiv:1702.06269*, 2017.
- [31] Yuhuai Wu, Elman Mansimov, Roger B Grosse, Shun Liao, and Jimmy Ba. Scalable trust-region method for deep reinforcement learning using kronecker-factored approximation. In *Advances in neural information processing systems*, pages 5285–5294, 2017.
- [32] Jian Zhang, Ioannis Mitliagkas, and Christopher Ré. Yellowfin and the art of momentum tuning. *arXiv preprint arXiv:1706.03471*, 2017.

A Derivation of generic update equations

In this section we will derive the generic IB update equations, starting from equation (5) and ending at equation (8). For notational simplicity we will drop superscripts and subscripts where they are clear from the context. Let a tilde denote the current iterate, i.e. $\tilde{\theta}_k = \theta_k^{(t)}$. With this notation, the IB update from (5) becomes

$$\begin{aligned} & \arg \min_{\theta} \left\{ 2\eta b^\top \sigma(\theta z) + \eta\mu \|\theta\|_2^2 + \|\theta - \tilde{\theta}\|_2^2 \right\} \\ &= \arg \min_{\theta} \left\{ \sum_{j=1}^{D_{k+1}} 2\eta b_j \sigma(\theta_j^\top z) + \eta\mu \|\theta\|_2^2 + \|\theta - \tilde{\theta}\|_2^2 \right\} \end{aligned} \quad (9)$$

where θ_j is the j^{th} row of θ corresponding to the j^{th} node in the layer. The minimization splits into separate minimization problems, one for each j :

$$\arg \min_{\theta_j} \left\{ 2\eta b_j \sigma(\theta_j^\top z) + \eta\mu \|\theta_j\|_2^2 + \|\theta_j - \tilde{\theta}_j\|_2^2 \right\}. \quad (10)$$

Since $\theta_j \in \mathbb{R}^{1+D_k}$ this is a $1 + D_k$ -dimensional problem. However, we will be able to reduce it to just a one-dimensional problem. We begin by introducing an auxiliary variable $q_j = \theta_j^\top z$ and rewriting (10) as

$$\min_{q_j} \left\{ 2\eta b_j \sigma(q_j) + \min_{\theta_j} \{ \eta\mu \|\theta_j\|_2^2 + \|\theta_j - \tilde{\theta}_j\|_2^2 : q_j = \theta_j^\top z \} \right\}. \quad (11)$$

We will first solve the inner minimization over θ_j as a function of q_j , and then solve the outer minimization over q_j .

Inner minimization

The inner minimization can be solved by taking the dual:

$$\begin{aligned} & \min_{\theta_j} \{ \eta\mu \|\theta_j\|_2^2 + \|\theta_j - \tilde{\theta}_j\|_2^2 : q_j = \theta_j^\top z \} \\ &= \max_{\lambda_j \in \mathbb{R}} \min_{\theta_j} \{ \eta\mu \|\theta_j\|_2^2 + \|\theta_j - \tilde{\theta}_j\|_2^2 + 2\lambda_j (q_j - \theta_j^\top z) \} \\ &= \max_{\lambda_j \in \mathbb{R}} \left\{ 2\lambda_j q_j + \min_{\theta_j} \{ \eta\mu \|\theta_j\|_2^2 + \|\theta_j - \tilde{\theta}_j\|_2^2 - 2\lambda_j \theta_j^\top z \} \right\}. \end{aligned} \quad (12)$$

The solution for θ_j is

$$\theta_j = \frac{\tilde{\theta}_j + \lambda_j z}{1 + \eta\mu}. \quad (13)$$

Substituting (13) into (12) and simplifying yields

$$- \frac{1}{1 + \eta\mu} \min_{\lambda_j \in \mathbb{R}} \left\{ \lambda_j^2 \|z\|_2^2 + 2\lambda_j (\tilde{\theta}_j^\top z - (1 + \eta\mu)q_j) - \eta\mu \|\tilde{\theta}_j\|_2^2 \right\}.$$

This is a quadratic in λ_j , which is easily minimized. The value for λ_j at the minimum is,

$$\lambda_j = \frac{(1 + \eta\mu)q_j - \tilde{\theta}_j^\top z}{\|z\|_2^2}. \quad (14)$$

Substituting (14) into (12) yields the minimal value of the inner minimization problem as a function of q_j ,

$$\frac{1 + \eta\mu}{\|z\|_2^2} \left(q_j - \frac{\tilde{\theta}_j^\top z}{1 + \eta\mu} \right)^2 + \frac{\eta\mu}{1 + \eta\mu} \|\tilde{\theta}_j\|_2^2. \quad (15)$$

Outer minimization

Replacing the inner minimization with (15), dropping the constant $\frac{\eta\mu}{1+\eta\mu}\|\tilde{\theta}_j\|_2^2$ term and dividing everything by 2η , (11) becomes

$$\arg \min_{q_j} \left\{ b_j \sigma(q_j) + \frac{1+\eta\mu}{2\eta\|z\|_2^2} \left(q_j - \frac{\tilde{\theta}_j^\top z}{1+\eta\mu} \right)^2 \right\}.$$

Reparameterizing q_j as

$$\alpha_j = \frac{1}{\eta\|z\|_2^2} \left(\frac{\tilde{\theta}_j^\top z}{1+\eta\mu} - q_j \right), \quad (16)$$

we arrive at our simplified update from (8):

$$\alpha_j = \arg \min_{\alpha} \left\{ b_j \cdot \sigma \left(\frac{\tilde{\theta}_j^\top z}{1+\eta\mu} - \alpha \cdot \eta\|z\|_2^2 \right) + \eta(1+\eta\mu)\|z\|_2^2 \frac{\alpha^2}{2} \right\}.$$

Once we have solved for α_j we can recover the optimal θ_j by using (16) to find q_j , (14) to find λ_j and (13) to find θ_j . The resulting formula is

$$\theta_j = \frac{\tilde{\theta}_j}{1+\eta\mu} - \eta\alpha_j z,$$

as was stated in (7).

B IB for convolutional neural networks

Here we consider applying IB to a Convolutional Neural Network (CNNs). As each filter is applied independently in a CNN, the IB updates decouple into separate updates for each filter. Since a filter uses shared weights, we cannot use the generic update equations in Section 4.1. Instead we have to derive the updates starting from (9)

$$\arg \min_{\theta} 2\eta b^\top \sigma(Z\theta) + \eta\mu\|\theta\|_2^2 + \|\theta - \tilde{\theta}\|_2^2. \quad (17)$$

Here Z is a matrix where each row corresponds to one patch over which the convolution vector θ is multiplied.⁹ The activation function σ has components $[\sigma(x)]_m = \max\{B_m x\}$ where B_m is a pooling matrix with elements in $\{0, 1\}$. We will assume that B_m has a row of all zeros so that the max-pooling effectively includes a relu non-linearity, since $\max\{(B_m^\top, 0)^\top x\} = \max\{\text{relu}(B_m x)\}$.

We can expand (17) into a quadratic program:

$$\begin{aligned} & \arg \min_{\theta} 2\eta \sum_{m=1}^M b_m \max\{B_m Z\theta\} + \eta\mu\|\theta\|_2^2 + \|\theta - \tilde{\theta}\|_2^2 \\ &= \arg \min_{a, \theta} 2\eta \sum_{m=1}^M |b_m| a_m + \eta\mu\|\theta\|_2^2 + \|\theta - \tilde{\theta}\|_2^2 \\ & \quad s.t. \quad a_m \geq \begin{cases} \max\{B_m Z\theta\} & \text{if } b_m \geq 0 \\ \min\{-B_m Z\theta\} & \text{if } b_m < 0 \end{cases} \\ &= \arg \min_{a, y, \theta} 2\eta \sum_{m=1}^M |b_m| a_m + \eta\mu\|\theta\|_2^2 + \|\theta - \tilde{\theta}\|_2^2 \\ & \quad s.t. \quad a_m \geq \begin{cases} B_m Z_j \theta & \text{if } b_m \geq 0 \\ -B_m Z_j \theta - M(1 - y_{mj}) & \text{if } b_m < 0 \end{cases} \quad \text{for all } j \\ & \quad \sum_j y_{mj} = 1 \\ & \quad y_{mj} \in \{0, 1\}, \end{aligned}$$

⁹Note that Z in general will have repeated entries and may have a column of ones appended to it to account for a bias.

where $M > 0$ is a large constant. This is clearly an expensive problem to solve each iteration.

Note that if the convolution did not include max-pooling, but just used shared weights, then the problem would become a quadratic program with continuous variables and no constraints, which could be solved analytically. On the other hand if the convolution had max-pooling, but no shared weights, then the generic IB updates from (7) would apply. Thus the difficulty in solving the IB convolutional update comes from doing the max-pooling and weight sharing in the *same* layer.

C Convergence theorem

In this section we present a simple theorem that leverages the fact that IB converges to EB in the limit of small learning rates, to show that IB converges to a stationary point of the loss function for appropriately decaying learning rates. First we will introduce some useful notation, after which we state the conditions under which the convergence theorem holds. After a few lemmas, we prove the desired result.

Notation. Let $g_i(\theta^{(t)}; \eta_t)$ denote the gradient used to take a step in IB when datapoint i is sampled with learning rate η , i.e. $\theta^{(t+1)} = \theta^{(t)} - \eta_t g_i(\theta^{(t)}; \eta_t)$. Let ℓ be the loss function from Sections 2 and 3. Define the level set

$$C = \{\theta : \|\theta\|_2^2 \leq \frac{2}{\mu} \ell(0)\}$$

and the restarting function

$$R(\theta) = \begin{cases} \theta & \text{if } \theta \in C \\ 0 & \text{otherwise.} \end{cases}$$

The set C depends on the value of $\ell(0)$. When $\theta = 0$ the output of the neural network is independent of its input and so $\ell(0) = \frac{1}{N} \sum_{i=1}^N \ell(y_i, f_0(x_i)) = \frac{1}{N} \sum_{i=1}^N \ell(y_i, f_0(0))$ can be quickly calculated. Finally define the extended level-set

$$\bar{C}(\eta) = \left\{ \theta : \|\theta\|_2 \leq \sqrt{\frac{2}{\mu} \ell(0) + \eta \cdot \max_{i, \theta \in C} \{ \|g_i(\theta; \eta)\|_2 \}} \right\}$$

to contain all points that can be reached from C in one IB iteration (without restarting).

We will assume the following conditions.

Assumption 1. The objective function $\ell(\theta) = \frac{1}{N} \sum_{i=1}^N \ell_\theta(x_i, y_i) + \frac{\mu}{2} \|\theta\|_2^2$, IB gradients $g_i(\theta^{(t)}; \eta)$ and learning rate sequence $\{\eta_t\}_{t=1}^\infty$ satisfy the following:

- (a) The loss at each datapoint is non-negative, i.e. $\ell_\theta(x, y) \geq 0$ for all x, y, θ .
- (b) The gradient function is Lipschitz continuous with a Lipschitz constant $0 < L(\eta) < \infty$ that is monotonically decreasing in η . That is

$$\|\nabla \ell(\theta) - \nabla \ell(\bar{\theta})\|_2 \leq L(\eta) \|\theta - \bar{\theta}\|_2,$$

for all $\{\theta, \bar{\theta}\} \subset \bar{C}(\eta)$ and $L(\eta) \leq L(\bar{\eta})$ if $\eta \leq \bar{\eta}$.

- (c) The gradients of the stochastic functions $\tilde{\ell}_k(\theta_k; x, y, \theta_{-k}^{(t)})$ in (3) are Lipschitz continuous with a Lipschitz constant $0 < \tilde{L}(\eta) < \infty$ that is monotonically decreasing in η . That is

$$\|\nabla \tilde{\ell}_k(\theta_k; x, y, \theta_{-k}^{(t)}) - \nabla \tilde{\ell}_k(\bar{\theta}_k; x, y, \theta_{-k}^{(t)})\|_2 \leq \tilde{L}(\eta) \|\theta_k - \bar{\theta}_k\|_2,$$

for all $k \in \{1, \dots, d\}$, $(x, y) \in \mathcal{D}$, $\theta^{(t)} \in C$ and $\{\theta, \bar{\theta}\} \subset \bar{C}(\eta)$; and $\tilde{L}(\eta) \leq \tilde{L}(\bar{\eta})$ if $\eta \leq \bar{\eta}$.

- (d) The learning rate sequence is monotonically decreasing with $\eta_1 \tilde{L}(\eta_1) < 1$, $\sum_{t=1}^\infty \eta_t = \infty$ and $\sum_{t=1}^\infty \eta_t^2 < \infty$.

A few comments on the assumptions. Assumption (a) is effectively equivalent to the loss being lower bounded by a deterministic constant $\ell_\theta(x, y) \geq B$, as one can always define an equivalent loss $\ell'_\theta(x, y) = \ell_\theta(x, y) - B \geq 0$. Most standard loss functions, such as the square loss, quantile loss, logistic loss and multinomial loss, satisfy assumption (a). Assumptions (b) and (c) will be valid for

any neural network whose activation functions have Lipschitz gradients. Assumption (d) is standard in SGD proofs (except for the $\eta_1 \tilde{L}(\eta_1) < 1$ assumption which is particular to us).

Let “restarting IB” refer to IB where the restarting operator R is applied each iteration. We now state the IB convergence theorem:

Theorem 1. *Under Assumptions 1, restarting IB converges to a stationary point in the sense that*

$$\lim_{T \rightarrow \infty} \frac{\sum_{t=1}^T \eta_t \mathbb{E}[\|\nabla \ell(\theta^{(t)})\|_2^2]}{\sum_{t=1}^T \eta_t} = 0.$$

The proof of Theorem 1 is given below, after a few helpful lemmas.

Lemma 1. *The restarting operator R does not increase the loss ℓ .*

Proof. If $\theta \in C$ then $\ell(R(\theta)) = \ell(\theta)$ and the loss stays the same, otherwise

$$\ell(R(\theta)) = \ell(0) < \frac{\mu}{2} \|\theta\|_2^2 \leq \ell(\theta),$$

where the first inequality is by the definition of C and the second is from the assumption that $\ell_\theta(x, y) \geq 0$. \square

Lemma 2. *The gradient of the loss function at any point in C is bounded by $B_\ell(\eta) = L(\eta) \sqrt{\frac{2}{\mu} \ell(0)} + \|\nabla \ell(0)\|_2$.*

Proof. By the triangle inequality and Lipschitz assumption

$$\begin{aligned} \|\nabla \ell(\theta)\|_2 &= \|\nabla \ell(\theta) - \nabla \ell(0) + \nabla \ell(0)\|_2 \\ &\leq \|\nabla \ell(\theta) - \nabla \ell(0)\|_2 + \|\nabla \ell(0)\|_2 \\ &\leq L(\eta) \|\theta - 0\|_2 + \|\nabla \ell(0)\|_2 \\ &\leq L(\eta) \sqrt{\frac{2}{\mu} \ell(0)} + \|\nabla \ell(0)\|_2 \\ &= B_\ell(\eta) \end{aligned}$$

for all $\theta \in C$. \square

Lemma 3. *If $\|x - y\|_2 \leq z$ then for any v we have $y^\top v \geq x^\top v - z\|v\|_2$.*

Proof.

$$\begin{aligned} y^\top v &\geq \min_s \{s^\top v : \|x - s\|_2^2 \leq z^2\} \\ &= \max_{\lambda \geq 0} \min_s \{s^\top v + \lambda(\|x - s\|_2^2 - z^2)\} \\ &= x^\top v - z\|v\|_2 \end{aligned}$$

where the final line follows from basic algebraic and calculus. \square

Lemma 4. *The 2-norm difference between the EB and IB gradients at $\theta^{(t)}$ with learning rate η_t is bounded by $\eta_t \tilde{L}(\eta_t) \|g_i(\theta^{(t)}; \eta_t)\|_2$.*

Proof. Let $\nabla \ell_{ik}(\theta)$ denote the components of $\nabla \ell_i(\theta)$ corresponding to the parameters of the k^{th} layer θ_k , i.e. $\nabla \ell_i(\theta) = (\nabla \ell_{i1}(\theta), \dots, \nabla \ell_{id}(\theta))$. By construction

$$\begin{aligned} \nabla \ell_{ik}(\theta^{(t)}) &= \nabla_{\theta_k} \tilde{\ell}_k(\theta_k; x, y, \theta_{-k}^{(t)}) \Big|_{\theta_k = \theta_k^{(t)}} \\ g_i(\theta^{(t)}; \eta_t) &= \nabla_{\theta_k} \tilde{\ell}_k(\theta_k; x, y, \theta_{-k}^{(t)}) \Big|_{\theta_k = \theta_k^{(t+1)}} \end{aligned}$$

where, in a slight abuse of notation, $\theta^{(t+1)}$ refers to the value of the next IB iterate *before* the application of the restarting operator. By the Lipschitz assumption on $\tilde{\ell}_k$ we have

$$\begin{aligned}
\|\nabla \ell_i(\theta^{(t)}) - g_i(\theta^{(t)}; \eta_t)\|_2^2 &= \sum_{k=1}^d \|\nabla \ell_{ik}(\theta^{(t)}) - g_{ik}(\theta^{(t)}; \eta_t)\|_2^2 \\
&= \sum_{k=1}^d \|\nabla_{\theta_k} \tilde{\ell}_k(\theta_k; x, y, \theta_{-k}^{(t)})|_{\theta_k=\theta_k^{(t)}} - \nabla_{\theta_k} \tilde{\ell}_k(\theta_k; x, y, \theta_{-k}^{(t)})|_{\theta_k=\theta_k^{(t+1)}}\|_2^2 \\
&\leq \sum_{k=1}^d \tilde{L}(\eta_t)^2 \|\theta_k^{(t)} - \theta_k^{(t+1)}\|_2^2 \\
&= \tilde{L}(\eta_t)^2 \|\theta^{(t)} - \theta^{(t+1)}\|_2^2 \\
&= \tilde{L}(\eta_t)^2 \|\eta_t g_i(\theta^{(t)}; \eta_t)\|_2^2 \\
&= \eta_t^2 \tilde{L}(\eta_t)^2 \|g_i(\theta^{(t)}; \eta_t)\|_2^2.
\end{aligned}$$

□

Lemma 5. *The 2-norm of the IB gradient $g_i(\theta; \eta_t)$ at any point in C is bounded by $B_g(\eta_t) = \frac{B_\ell(\eta_t)}{1 - \eta_t \tilde{L}(\eta_t)}$.*

Proof. By Lemmas 2, 4 and the triangle inequality,

$$\begin{aligned}
\|g_i(\theta; \eta_t)\|_2 &= \|g_i(\theta; \eta_t) - \nabla \ell_i(\theta) + \nabla \ell_i(\theta)\|_2 \\
&\leq \|g_i(\theta; \eta_t) - \nabla \ell_i(\theta)\|_2 + \|\nabla \ell_i(\theta)\|_2 \\
&\leq \eta_t \tilde{L}(\eta_t) \|g_i(\theta; \eta_t)\|_2 + B_\ell(\eta_t).
\end{aligned} \tag{18}$$

Note that $\eta_1 \tilde{L}(\eta_1) < 1$ by assumption. Since $\eta_t \leq \eta_1$ and $\tilde{L}(\eta)$ is monotonically decreasing in η , we have that $\eta_t \tilde{L}(\eta_t) < 1$ for all $t \geq 1$. Thus subtracting $\eta_t \tilde{L}(\eta_t) \|g_i(\theta; \eta_t)\|_2$ from both sides of (18) and dividing by $1 - \eta_t \tilde{L}(\eta_t) > 0$ yields the desired result. □

Proof of Theorem 1. We upper bound the loss of restarting-IB as

$$\begin{aligned}
\mathbb{E}[\ell(\theta^{(t+1)})] &= \mathbb{E}[\ell(R(\theta^{(t)} - \eta_t g_i(\theta^{(t)}; \eta_t)))] \\
&\leq \mathbb{E}[\ell(\theta^{(t)} - \eta_t g_i(\theta^{(t)}; \eta_t))] \\
&\leq \mathbb{E}[\ell(\theta^{(t)}) - \eta_t g_i(\theta^{(t)}; \eta_t)^\top \nabla \ell(\theta^{(t)}) + \frac{1}{2} \eta_t^2 L(\eta) \|g_i(\theta^{(t)}; \eta_t)\|_2^2] \\
&= \mathbb{E}[\ell(\theta^{(t)})] - \eta_t \mathbb{E}[g_i(\theta^{(t)}; \eta_t)^\top \nabla \ell(\theta^{(t)})] + \frac{1}{2} \eta_t^2 L(\eta) \mathbb{E}[\|g_i(\theta^{(t)}; \eta_t)\|_2^2].
\end{aligned} \tag{19}$$

Lets focus on the second term in (19), $\mathbb{E}[g_i(\theta^{(t)}; \eta_t)^\top \nabla \ell(\theta^{(t)})]$. By Lemmas 3 and 4 we have that

$$g_i(\theta^{(t)}; \eta_t)^\top \nabla \ell(\theta^{(t)}) \geq \nabla \ell_i(\theta^{(t)})^\top \nabla \ell(\theta^{(t)}) - \eta_t \tilde{L}(\eta) \|g_i(\theta^{(t)}; \eta_t)\|_2 \|\nabla \ell(\theta^{(t)})\|_2$$

and so

$$\begin{aligned}
\mathbb{E}[g_i(\theta^{(t)}; \eta_t)^\top \nabla \ell(\theta^{(t)})] &\geq \|\nabla \ell(\theta^{(t)})\|_2^2 - \eta_t \tilde{L}(\eta) \mathbb{E}[\|g_i(\theta^{(t)}; \eta_t)\|_2] \|\nabla \ell(\theta^{(t)})\|_2 \\
&\geq \|\nabla \ell(\theta^{(t)})\|_2^2 - \eta_t \tilde{L}(\eta) B_g(\eta_t) B_\ell(\eta_t)
\end{aligned}$$

where $B_\ell(\eta_t)$ is as defined in Lemma 2 and $B_g(\eta_t)$ in Lemma 5. Moving onto the third term in (19), we have

$$\mathbb{E}[\|g_i(\theta^{(t)}; \eta_t)\|_2^2] \leq B_g^2(\eta_t)$$

by Lemma 5. Putting all the terms in (19) together

$$\begin{aligned}
\mathbb{E}[\ell(\theta^{(t+1)})] &\leq \mathbb{E}[\ell(\theta^{(t)})] - \eta_t (\|\nabla \ell(\theta^{(t)})\|_2^2 - \eta_t \tilde{L}(\eta_t) B_g(\eta_t) B_\ell(\eta_t)) + \frac{1}{2} \eta_t^2 L(\eta_t) B_g^2(\eta_t) \\
&= \mathbb{E}[\ell(\theta^{(t)})] - \eta_t \|\nabla \ell(\theta^{(t)})\|_2^2 + \eta_t^2 (\tilde{L}(\eta_t) B_g(\eta_t) B_\ell(\eta_t) + \frac{1}{2} L(\eta_t) B_g^2(\eta_t)) \\
&\leq \mathbb{E}[\ell(\theta^{(t)})] - \eta_t \|\nabla \ell(\theta^{(t)})\|_2^2 + \eta_t^2 (\tilde{L}(\eta_1) B_g(\eta_1) B_\ell(\eta_1) + \frac{1}{2} L(\eta_1) B_g(\eta_1)^2)
\end{aligned}$$

where we have used the assumption that L and \tilde{L} are monotonically decreasing in η (that B_ℓ and B_g are also monotonically decreasing in η follows from the assumptions on L and \tilde{L}). Using a telescoping sum and rearranging yields

$$\begin{aligned} \sum_{t=1}^T \eta_t \mathbb{E}[\|\nabla \ell(\theta^{(t)})\|_2^2] &\leq \mathbb{E}[\ell(\theta^{(1)})] - \mathbb{E}[\ell(\theta^{(T+1)})] \\ &\quad + (\tilde{L}(\eta_1)B_g(\eta_1)B_\ell(\eta_1) + \frac{1}{2}L(\eta_1)B_g(\eta_1)^2) \sum_{t=1}^T \eta_t^2 \\ &\leq \mathbb{E}[\ell(\theta^{(1)})] + (\tilde{L}(\eta_1)B_g(\eta_1)B_\ell(\eta_1) + \frac{1}{2}L(\eta_1)B_g(\eta_1)^2) \sum_{t=1}^T \eta_t^2 \end{aligned} \quad (20)$$

where the second inequality follows from the assumption that $\ell(\theta) \geq 0$. Both of the terms in (20) are deterministically bounded for all T and so it must be the case that

$$\sum_{t=1}^{\infty} \eta_t \mathbb{E}[\|\nabla \ell(\theta^{(t)})\|_2^2] < \infty.$$

Finally, by the assumption that $\sum_{t=1}^{\infty} \eta_t = \infty$ we have

$$\lim_{T \rightarrow \infty} \frac{\sum_{t=1}^T \eta_t \mathbb{E}[\|\nabla \ell(\theta^{(t)})\|_2^2]}{\sum_{t=1}^T \eta_t} = 0.$$

□

D Experimental setup

In this section we describe the datasets, hyperparameters, run times and results of the experiments from Section 5 in greater detail.

D.1 Datasets

The experiments use three types of dataset: MNIST for image classification and autoencoding, 4 polyphonic music dataset for RNN prediction and 121 UCI datasets for classification. These are standard benchmark datasets that are often used in the literature: MNIST is arguably the most used dataset in machine learning [16], the polyphonic music datasets are a standard for testing real world RNNs [19, 21, 4] and the UCI datasets are an established benchmark for comparing the performance of classification algorithms [9, 14].

The sources of the datasets are given in Table 2 along with a basic description of their characteristics in Table 3. The MNIST and UCI datasets were pre-split into training and test sets. For the music datasets we used a random 80%-20% train-test split.

Table 2: Data sources

Dataset	Source url
MNIST	http://yann.lecun.com/exdb/mnist/
Polyphonic music	http://www-etud.iro.umontreal.ca/~boulanni/icml2012 .
UCI classification	https://github.com/bioinf-jku/SNNs .

D.2 Loss metrics

For all of the experiments we used standard loss metrics. For image classification we used the cross-entropy and for autoencoders the mean squared error. As suggested by Boulanger-Lewandowski et al. [4] on their website <http://www-etud.iro.umontreal.ca/~boulanni/icml2012>, we used the expected frame level accuracy as the loss for the music prediction problems. That is, at each time

Table 3: Data characteristics. An asterisk * indicates the average length of the musical piece. 88 is the number of potential notes in each chord. For information on the UCI classification datasets, see [14, Appendix 4.2].

Dataset	Train	Test	Dimension	Classes
MNIST	60,000	10,000	28x28	10
JSB Chorales	229 (60*)	77 (61*)	88	88
MuseData	524 (468*)	124 (519*)	88	88
Nottingham	694 (254*)	170 (262*)	88	88
Piano-midi.de	87 (873*)	25 (761*)	88	88

step the RNN outputs a vector in $[0, 1]^{88}$ representing the probability of each of the 88 notes in the next chord being played or not. This naturally defines a likelihood of the next chord. We use the log of this likelihood as our loss. Also as suggested by Boulanger-Lewandowski et al. [4], the loss for each piece is divided by its length, so that the loss is of similar magnitude for all pieces.

D.3 Architectures

We endeavored to use standard architectures so that the experiments would be a fair representation how the algorithms might perform in practical applications. The architecture for each type of dataset is given below.

MNIST classification. The architecture is virtually identical to that given in the MNIST classification Pytorch tutorials available at <https://github.com/pytorch/examples/blob/master/mnist/main.py>. The input is a 28×28 dimensional image. We first apply two 2d-convolutions with a relu activation function and max-pooling. The convolution kernel size is 5 with 10 filters for the first convolution and 20 filters for the second, and the max-pooling kernel size is 2. After that we apply one arctan layer with input size 320 and output size 50, followed by dropout at a rate of 0.5 and a relu layer with output size 10. This is fed into the softmax function to get probabilities over the 10 classes.

Since IB is not applicable to convolutional layers, for the IB implementation we use EB updates for the convolutional layers and IB for the arctan and relu layers. For the EB implementation, we use EB updates for all of the layers.

MNIST autoencoder. The autoencoder architecture just involves relus and has a 784:500:300:100:30:100:300:500:784 structure. This is similar to, but deeper than, the structure used in [18].

Music prediction. The simple RNN architecture used is identical to that in [21], except for the fact that we use an arctan activation function instead of tanh (since IB is compatible with arctan but not with tanh). 300 hidden units are used.

UCI datasets. The architecture used for the UCI datasets consists of three arctan layers followed by a linear layer and the softmax. The number of nodes in the arctan layers are equal to the number of features in the dataset, with the final linear layer having input size equal to the number of features and output size equal to the number of classes. This architecture is based on [14], who also use the same UCI datasets with a similar architecture.

D.4 Hyperparameters and initialization details

The hyperparameters and parameter initializations schemes used are as follows:

- Batch size: 100 (except for RNNs which had a batch-size of 1)
- Dropout: None (unless otherwise stated)
- Momentum: None

- Ridge-regularization (μ): 0
- Weight matrix initialization: Each element is sampled independently from $unif\left(-\sqrt{\frac{6}{n+m}}, \sqrt{\frac{6}{n+m}}\right)$, where n = input size, m = output size to layer. This follows advice of [10, p. 299]
- Bias initialization: 0. Again, this follows advice of [10, p. 299]

D.5 Learning rates

The process used to decide on the learning rates for the MNIST and music experiments is as follows. First a very coarse grid of learning rates was tested using EB to ascertain the range of learning rates where EB performed reasonably well. We then constructed a finer grid of learning rates around where EB performed well. The finer grid was constructed so that EB demonstrated in a U-shape of losses, with lower and higher learning rates having higher losses than learning rates in the middle, as in [10, Fig 11.1, p. 425]. It was this finer grid that was used to generate the final results. Note that at no stage was IB involved in constructing the grid and thus, if anything, the grid is biased in favor of EB.

For the UCI datasets the following set of learning rates were used: 0.001, 0.01, 0.1, 0.5, 1.0, 3.0, 5.0, 10.0, 30.0, 50.0. This is quite a coarse grid over a very large range of values.

D.6 Clipping

Clipping was not used except for those experiments where the effect of clipping was explicitly being investigated. When clipping was used, the gradients were clipping according to their norm (opposed to each component being clipped separately). For EB we applied clipping in the usual way: first calculating the gradient, clipping it and then taking the step using the clipped gradient. To implement clipping for IB we used an alternative definition of the IB step from (1): $\theta^{(t+1)} = \theta^{(t)} - \eta_t(\nabla_{\theta} \ell_i(\theta^{(t+1)}) + \mu\theta^{(t+1)})$, where we highlight that the gradient is evaluated at the next, not current, value of θ . The IB gradient can be inferred using

$$\nabla_{\theta} \ell_i(\theta^{(t+1)}) + \mu\theta^{(t+1)} = (\theta^{(t)} - \theta^{(t+1)})/\eta_t \quad (21)$$

where $\theta^{(t+1)}$ is calculated using (4). When applying clipping to IB we first calculate $\theta^{(t+1)}$ using the IB update, infer the IB gradient using (21), clip it, and finally take a step equal to the learning rate multiplied by the clipped gradient.

E Results

Here we will give the full results of all of the experiments. We begin with giving the run times of each experiment after which we present the performance on the MNIST and music datasets. Finally we give results on the UCI datasets.

E.1 Run times

In Section 4.5 upper bounds on the relative increase in run time for IB as compared to EB were derived. The bounds for each experiment are displayed in Table 4 along with the empirically measured relative run times of our basic Pytorch implementation. The Pytorch run times are higher than in the theoretical upper bounds. This shows that IB could be more efficiently implemented.

E.2 Results from MNIST and music experiments

In this section the plots for all of the experiments are presented. For each experiment we have multiple plots: a line plot showing the mean performance along with 1 standard deviation error bars; a scatter plot showing the performance for each random seed; and, where applicable, line and scatter plots showing the difference between the experiment with and without clipping. In general 5 seeds are used per learning rate, although for MNIST-classification we use 20 seeds.

Table 4: Theoretical and empirical relative run time of IB vs EB. Empirical measured on AWS p2.xlarge with our basic Pytorch implementation.

Dataset	Theoretical upper bound	Empirical
MNIST classification	6.27%	16.82%
MNIST autoencoder	0.60%	99.68%
JSB Chorals	11.33%	152.51%
MuseData	11.33%	207.48%
Nottingham	11.33%	215.85%
Piano-midi.de	11.33%	213.98%
UCI classification sum	-	58.99%

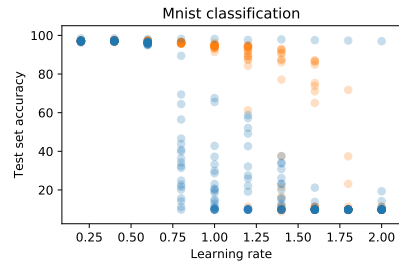
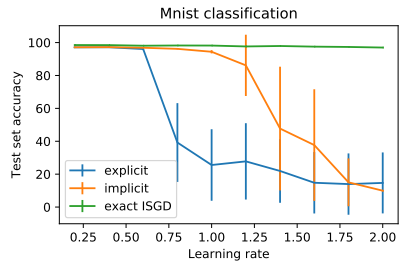
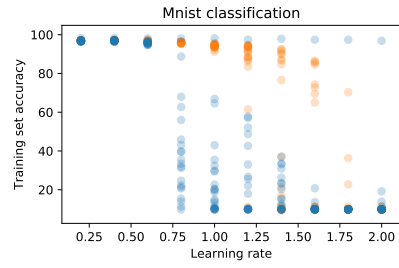
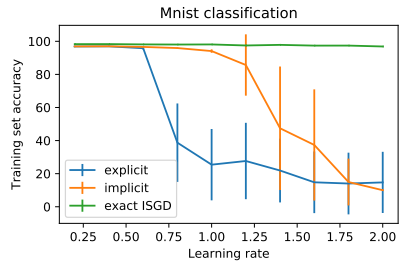
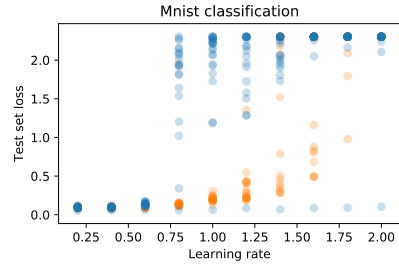
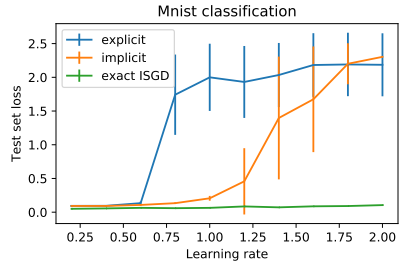
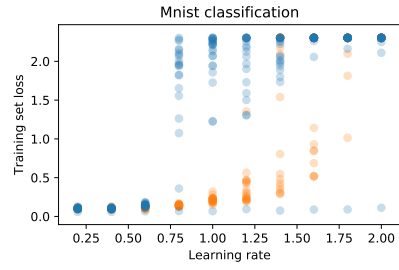
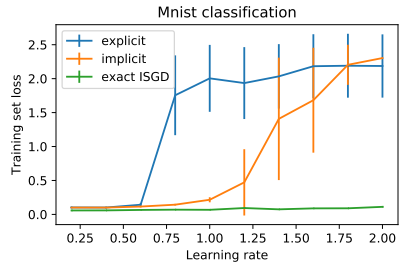
The experiments are presented in the following order

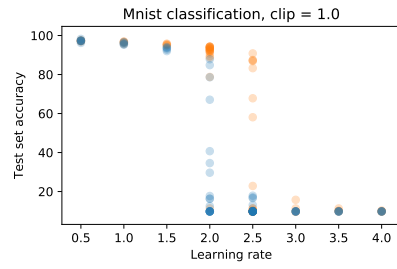
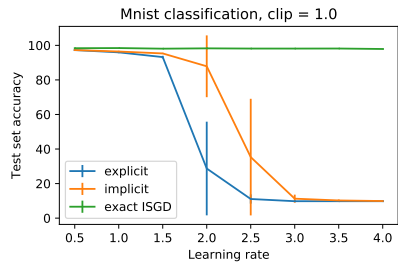
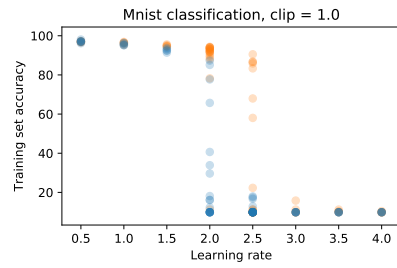
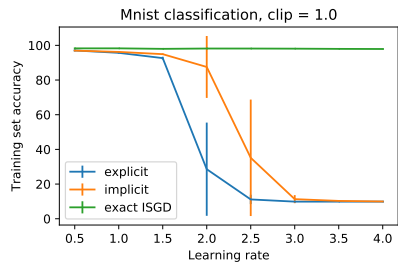
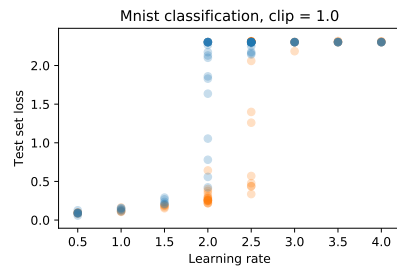
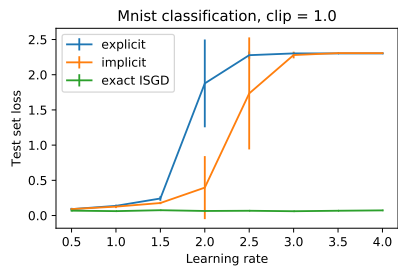
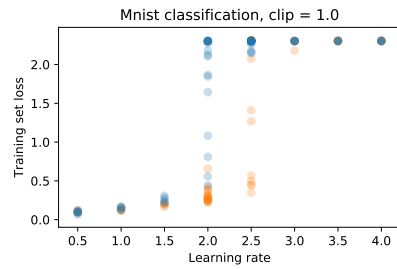
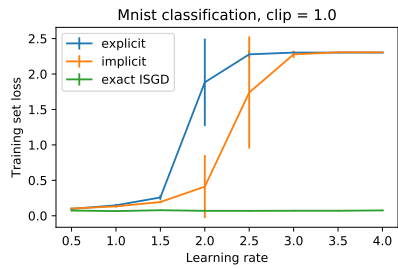
1. MNIST classification without clipping
2. MNIST classification with clipping threshold = 1.0
3. MNIST autoencoder without clipping
4. MNIST autoencoder with clipping threshold = 1.0
5. JSB Chorales without clipping
6. JSB Chorales with clipping threshold = 8.0
7. JSB Chorales with clipping threshold = 1.0
8. JSB Chorales with clipping threshold = 0.1
9. MuseData without clipping
10. MuseData with clipping threshold = 8.0
11. Nottingham without clipping
12. Nottingham with clipping threshold = 8.0
13. Piano-midi.de without clipping
14. Piano-midi.de with clipping threshold = 8.0
15. Piano-midi.de with clipping threshold = 1.0
16. Piano-midi.de with clipping threshold = 0.1
17. Piano-midi.de with clipping threshold = 0.01

For the MNIST experiments we only used a clipping threshold of 1.0. For the music datasets we first use a clipping threshold of 8.0 as suggested by the authors of [21]. As this clipping threshold didn't much affect the performance of either EB or IB, we also considered lower clipping thresholds.

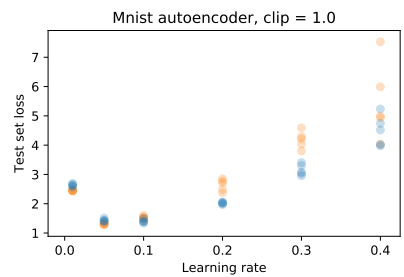
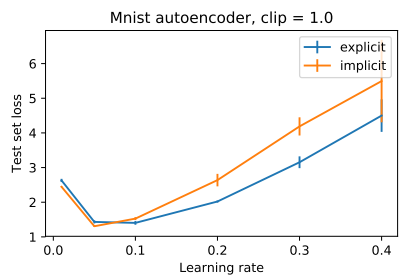
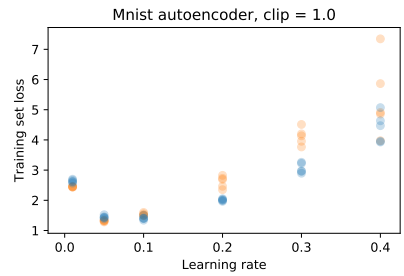
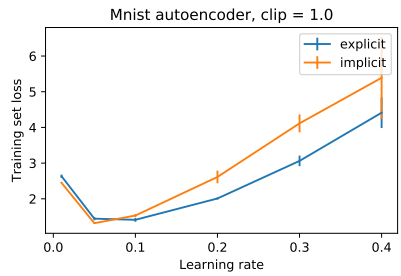
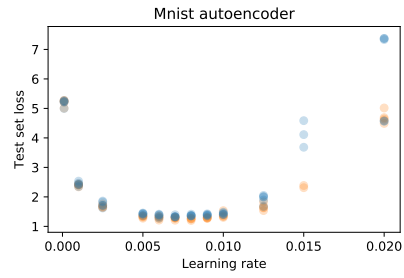
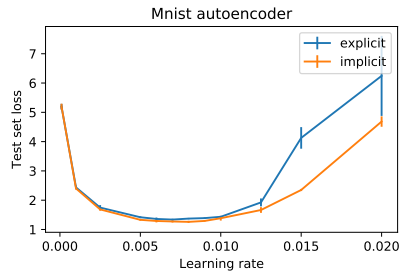
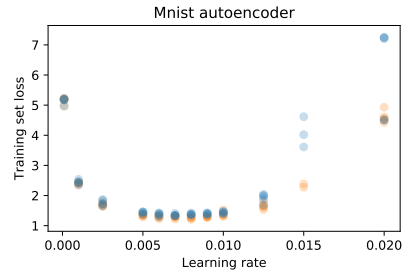
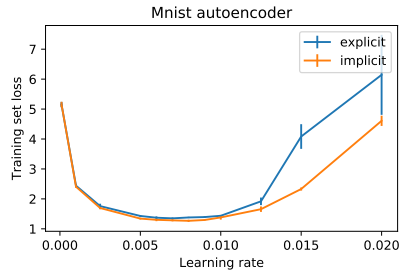
It is evident from the plots without clipping that on Piano-midi.de the algorithms are less well converged than the other datasets (which is probably due to Piano-midi.de having only 87 training datapoints). It was therefore of interest to see if further clipping could help stabilize the algorithms on Piano-midi.de. We can see from the random seed scatter plots that the effect of clipping helped a little with stabilization, but not to the extent that the results were significantly better. As JSB Chorales has the second fewest number of datapoints, we also tried lower clipping thresholds on it, and found it to often hurt the performance of EB as much as it helped (depending on the random seed).

E.3 MNIST classification

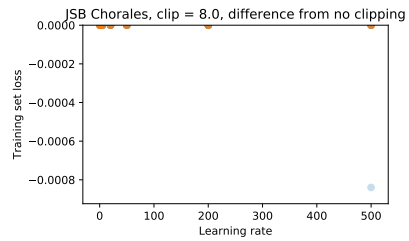
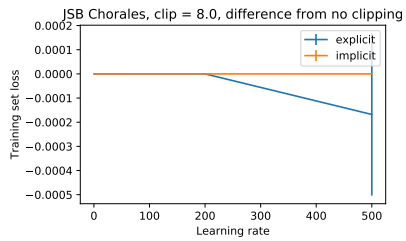
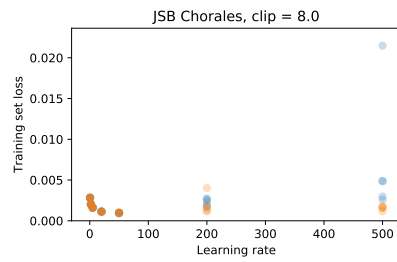
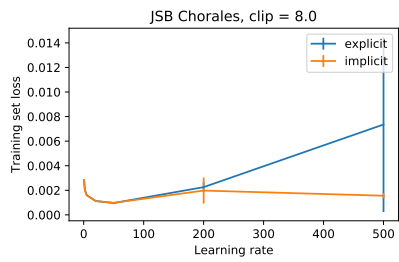
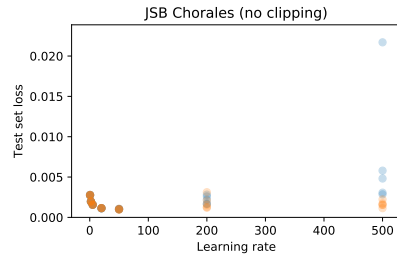
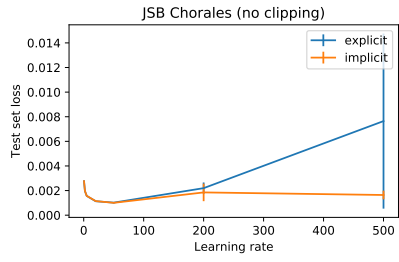
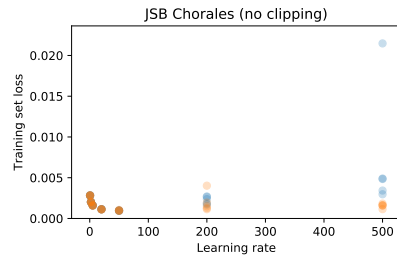
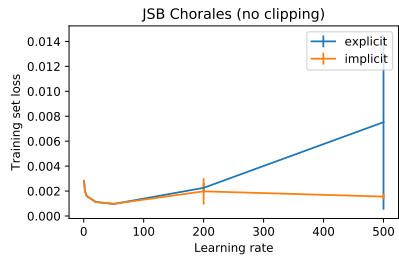


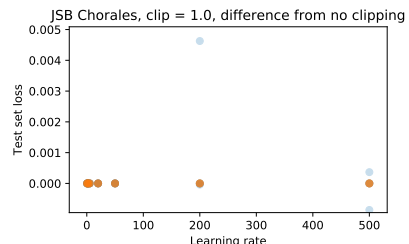
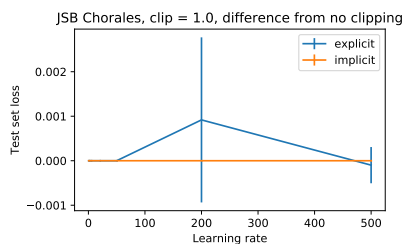
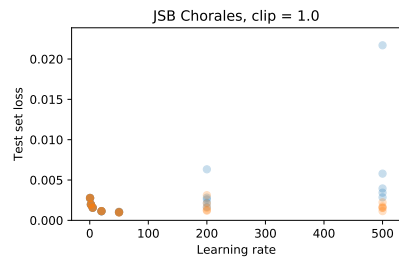
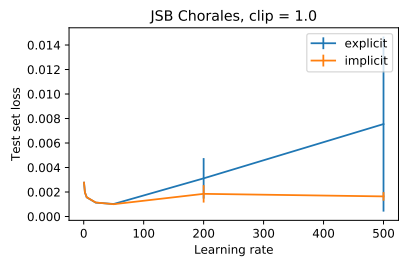
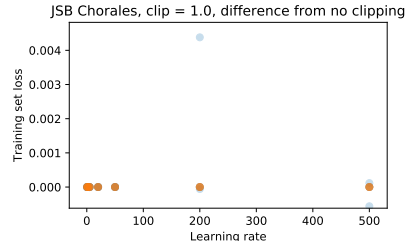
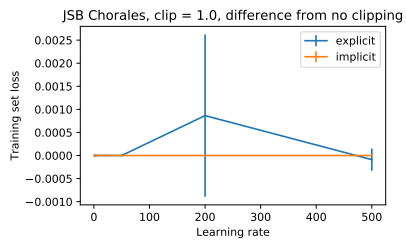
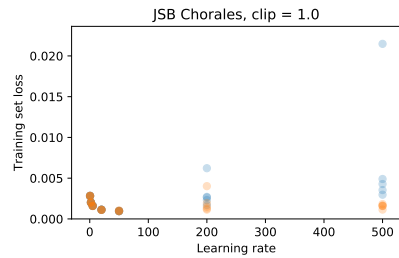
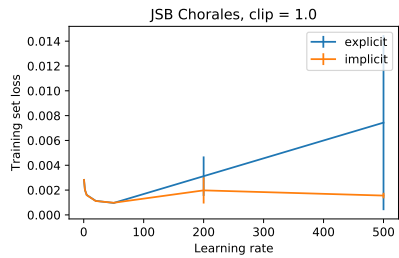
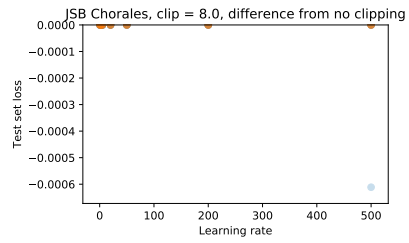
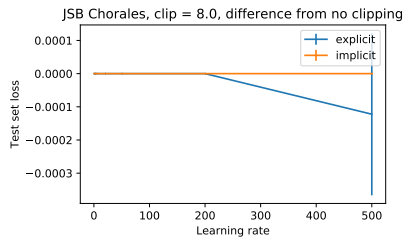
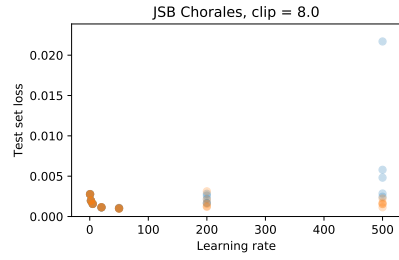
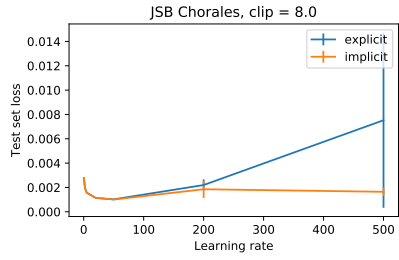


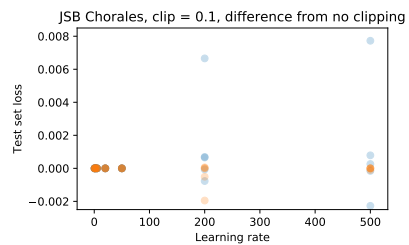
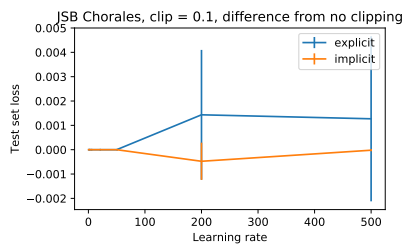
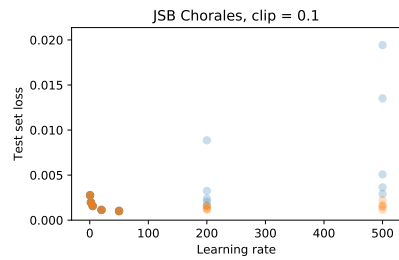
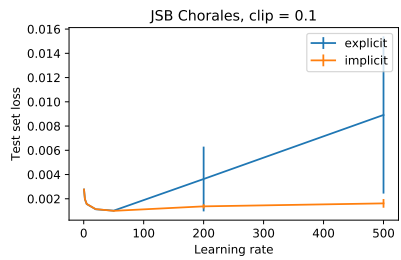
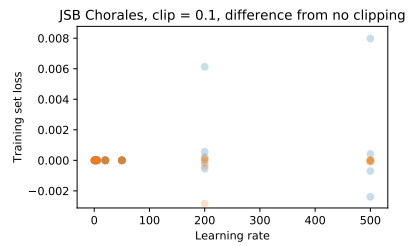
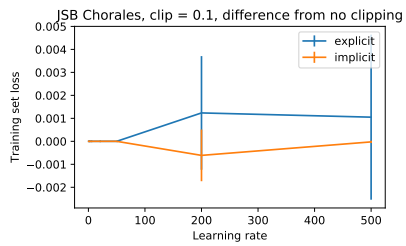
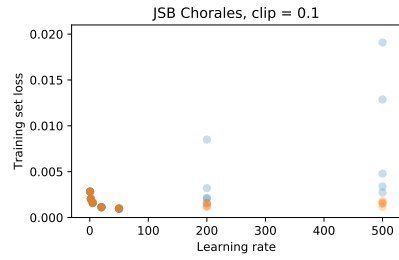
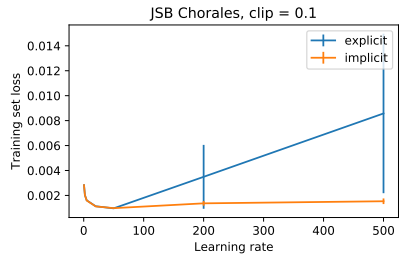
E.4 MNIST autoencoder



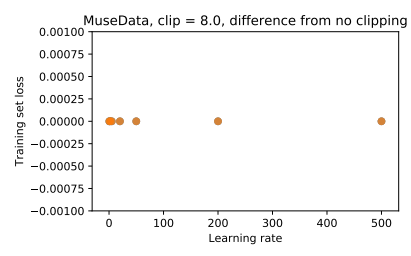
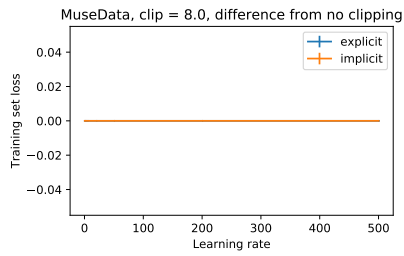
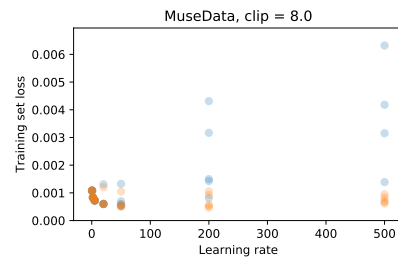
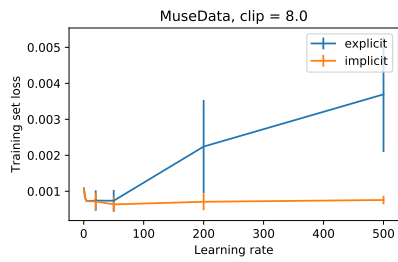
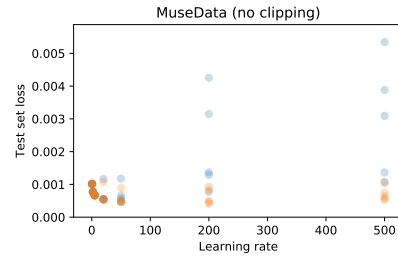
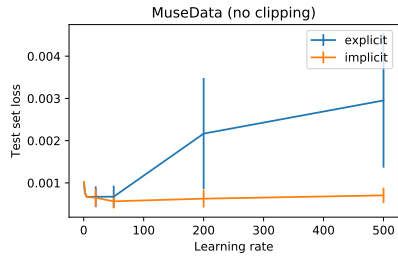
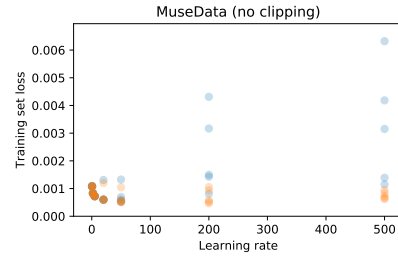
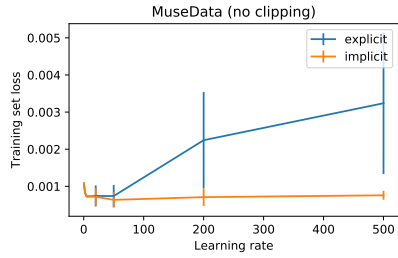
E.5 JSB Chorales

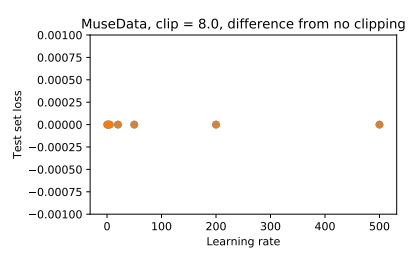
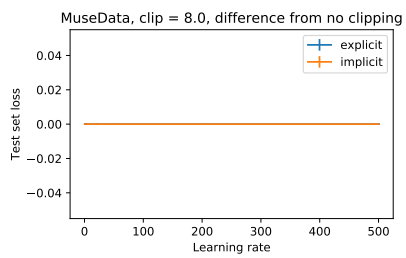
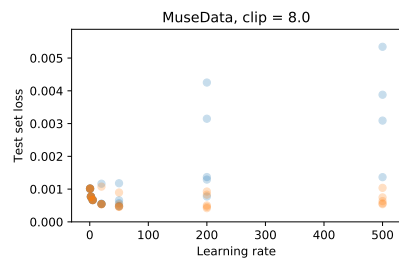
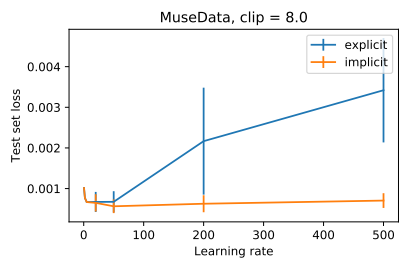




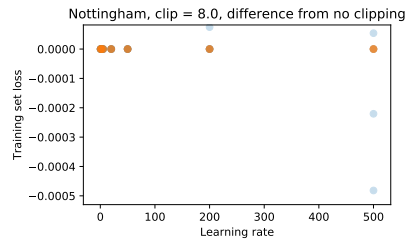
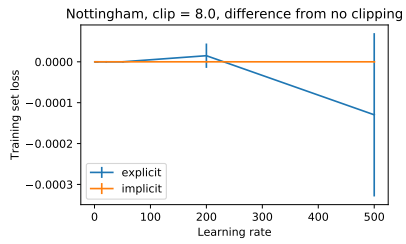
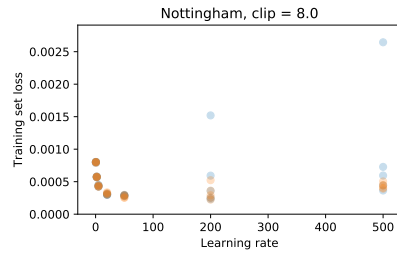
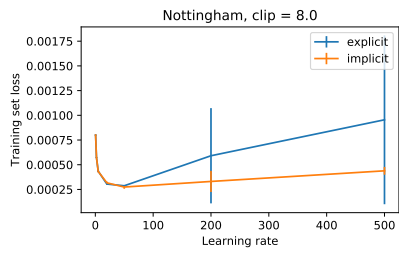
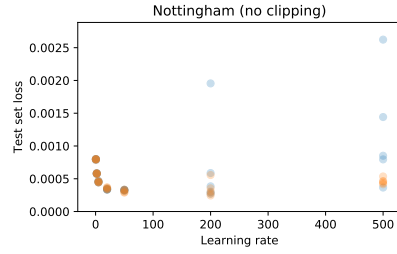
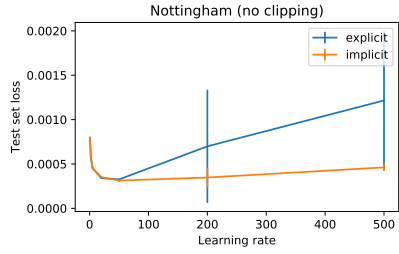
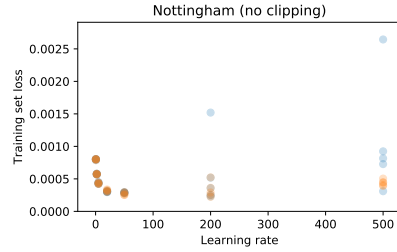
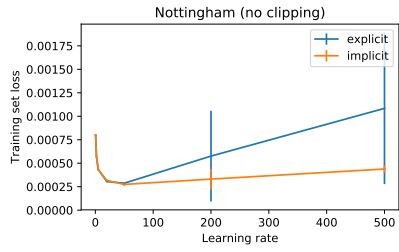


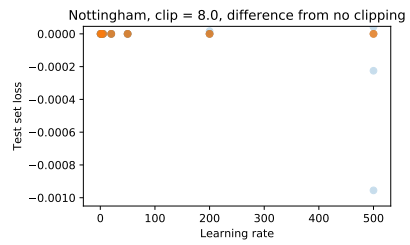
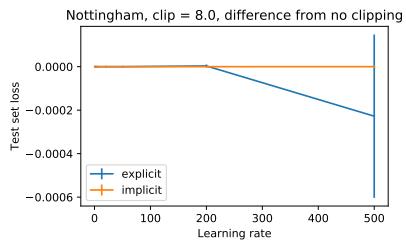
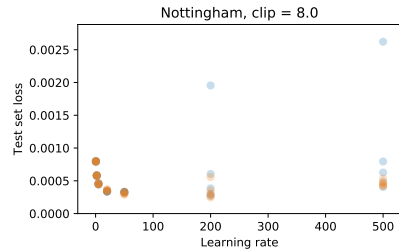
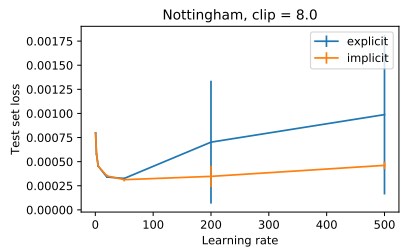
E.6 MuseData



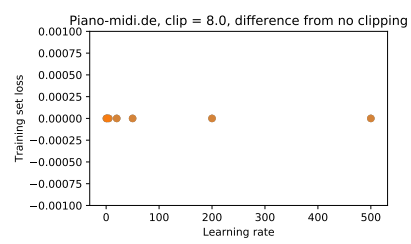
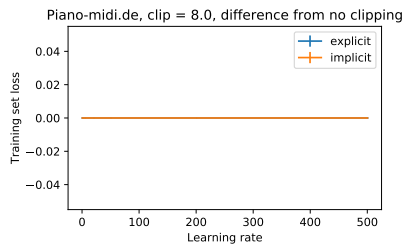
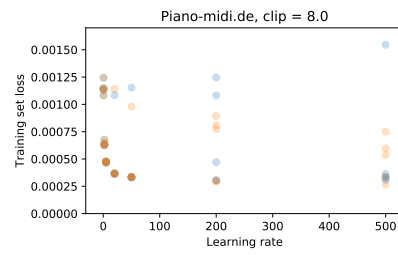
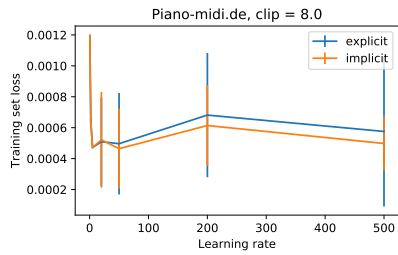
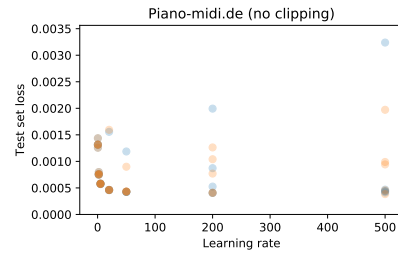
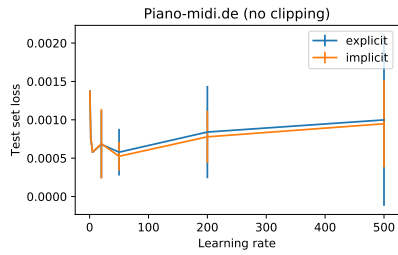
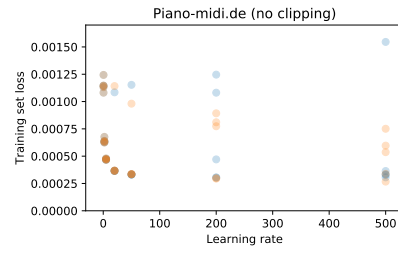
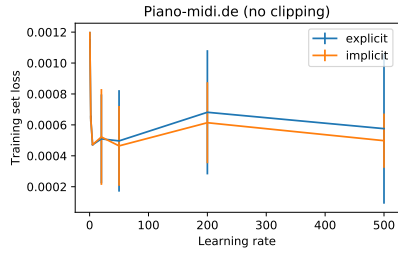


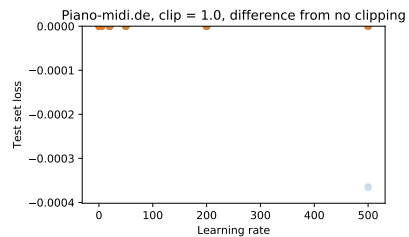
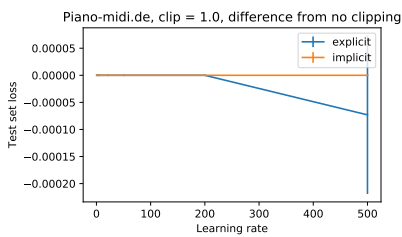
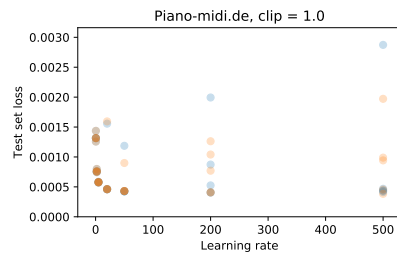
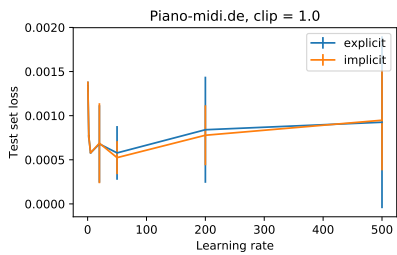
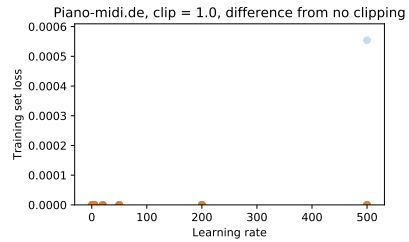
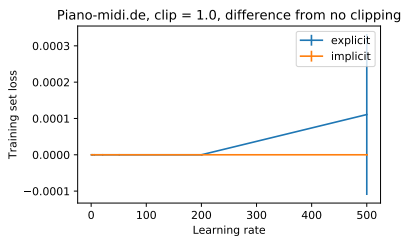
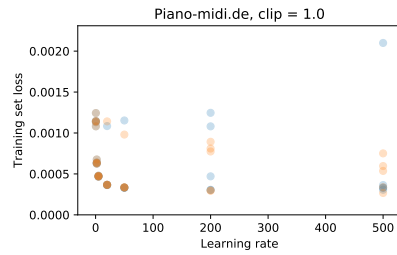
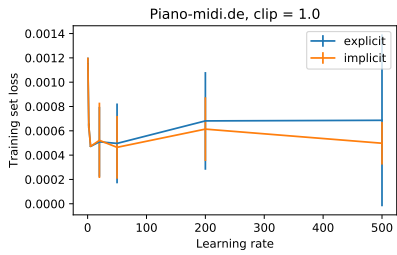
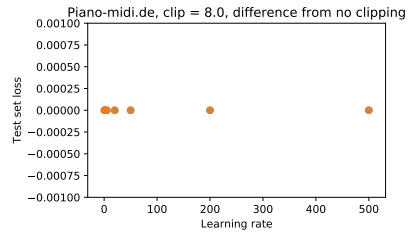
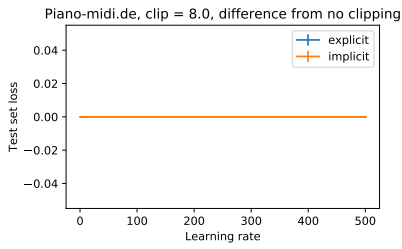
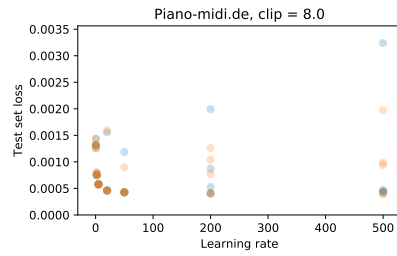
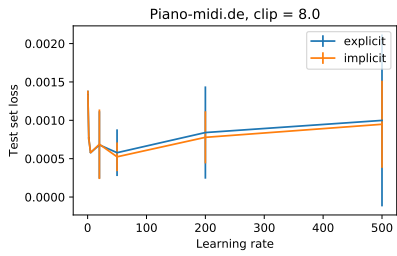
E.7 Nottingham

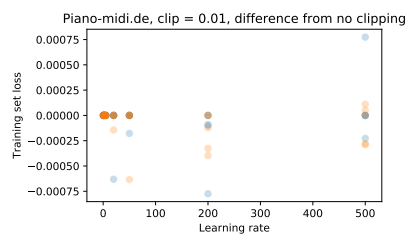
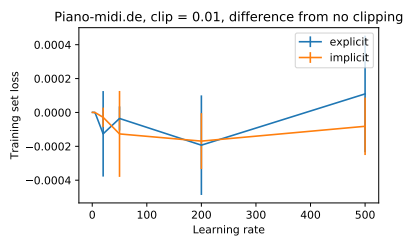
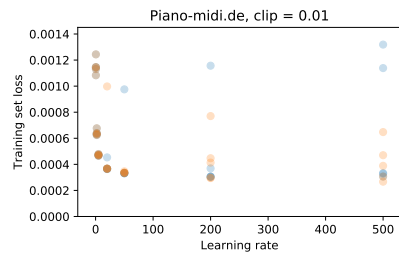
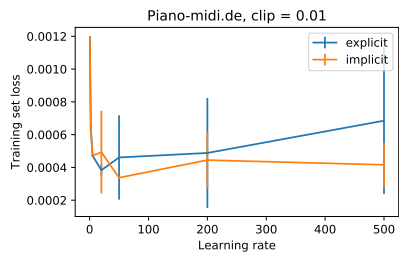
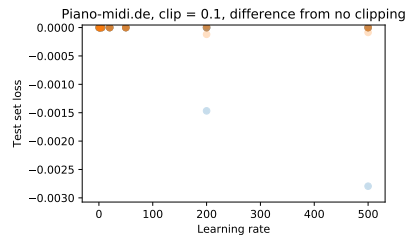
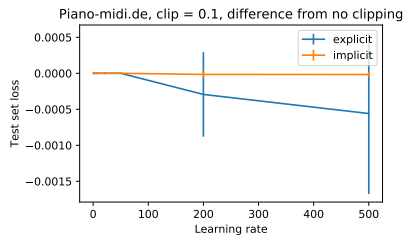
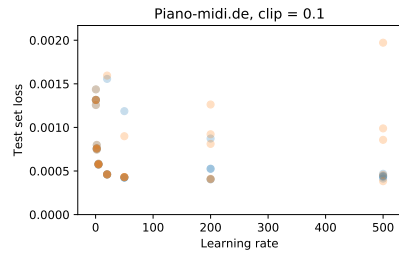
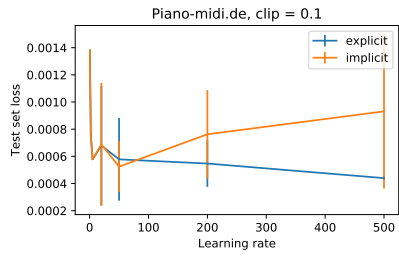
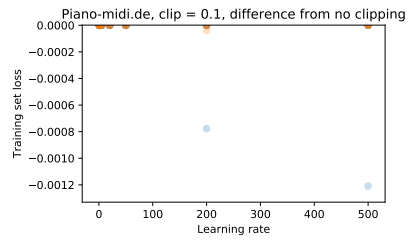
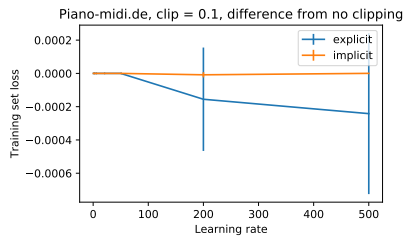
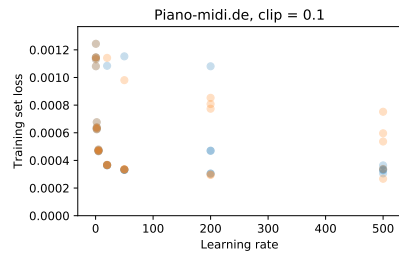
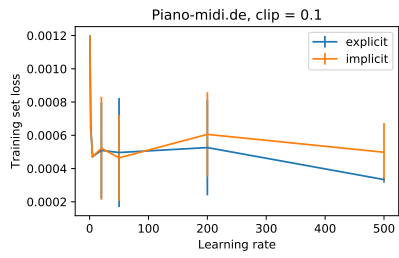


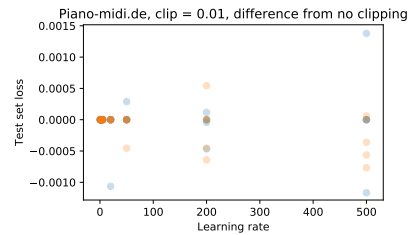
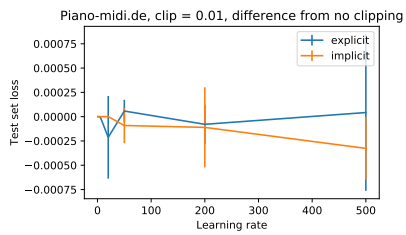
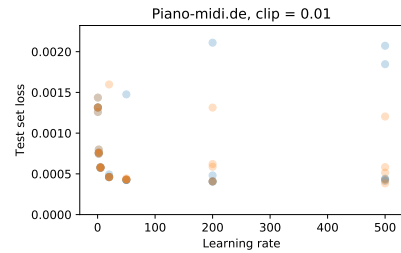
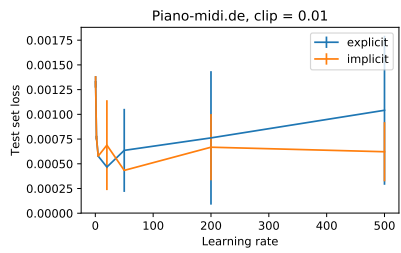


E.8 Piano-midi.de

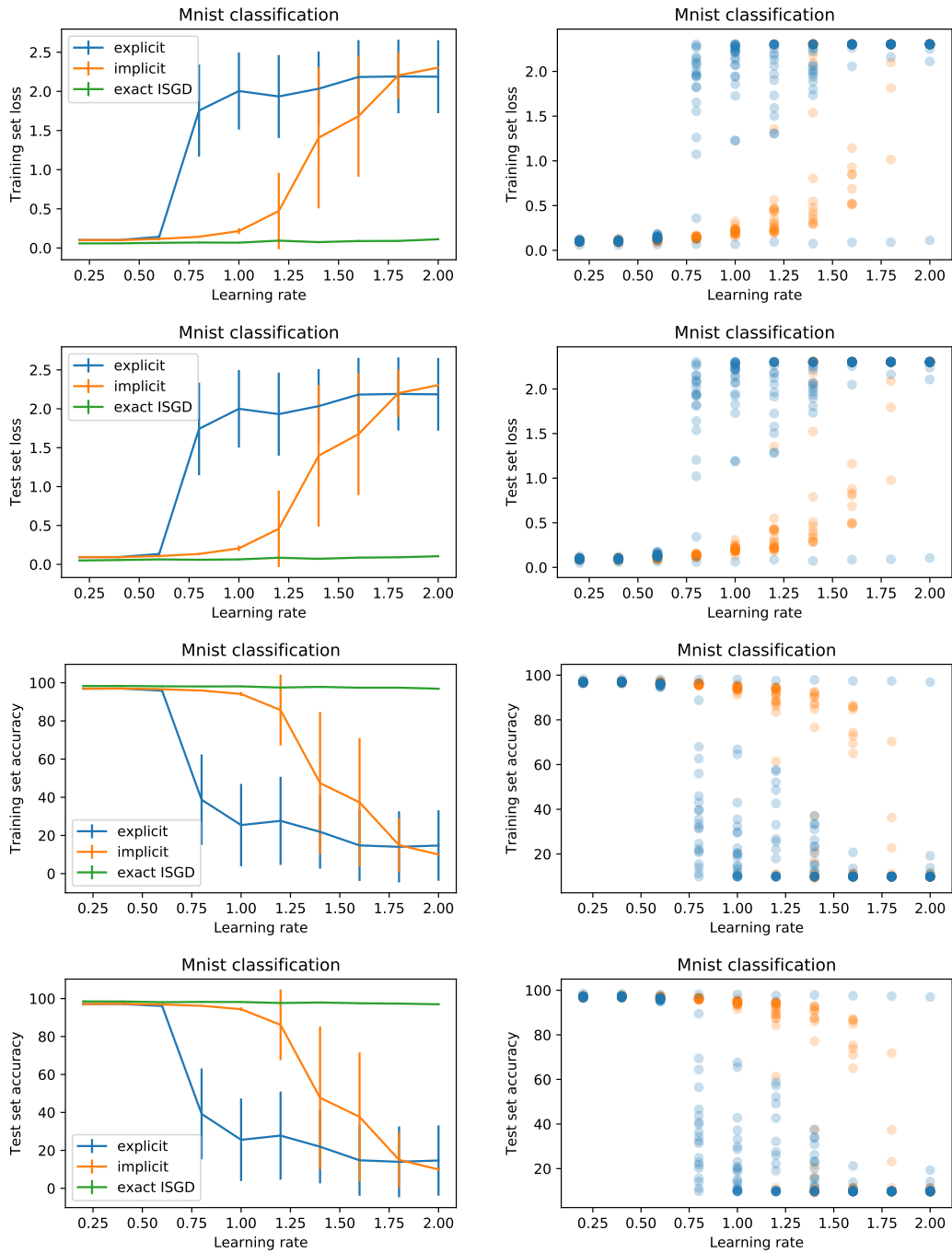


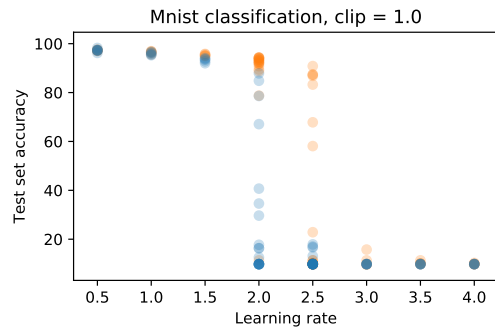
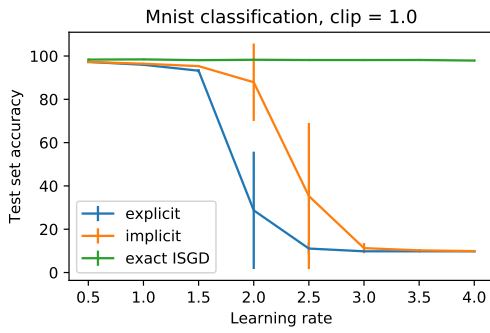
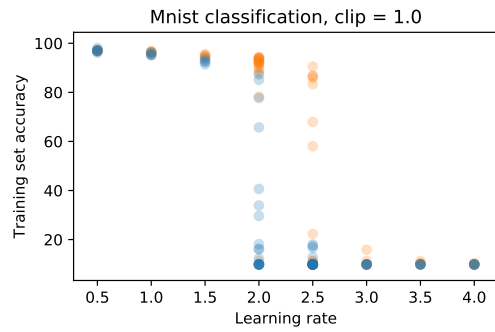
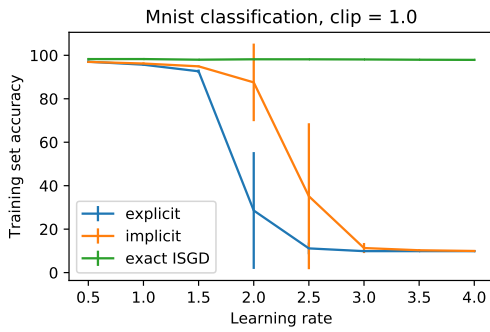
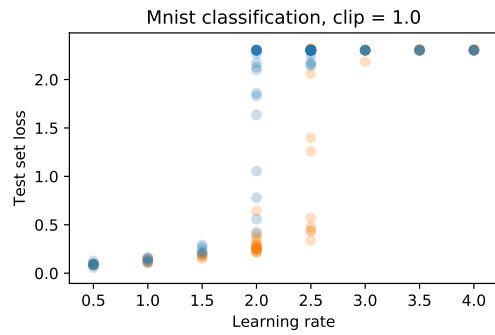
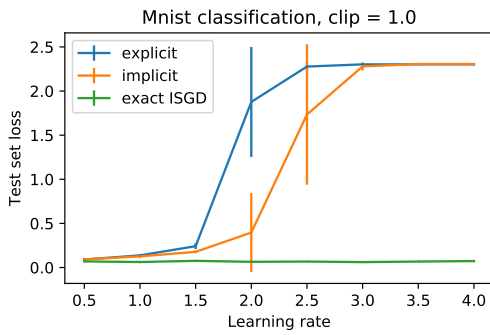
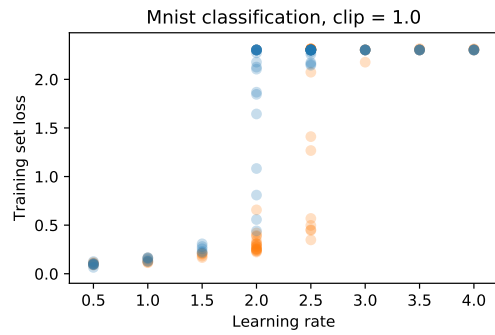
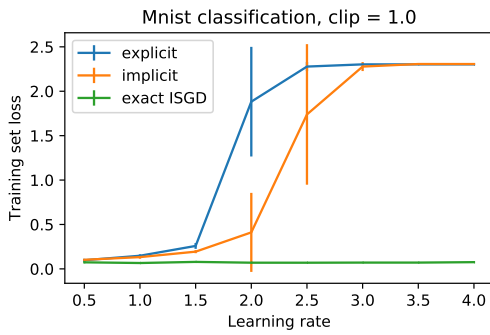




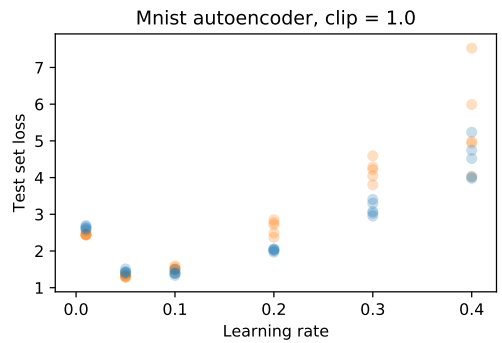
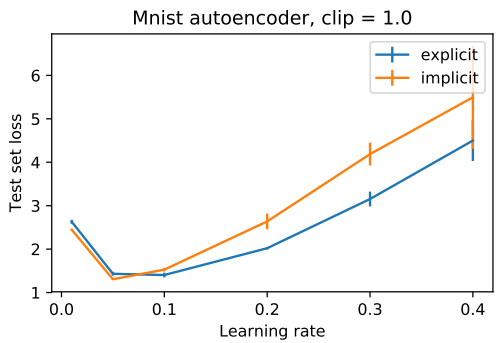
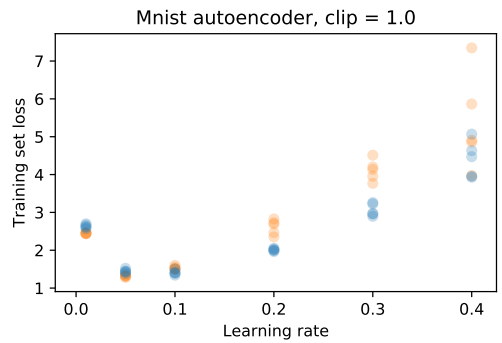
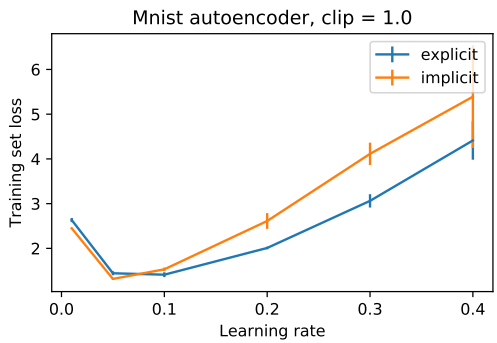
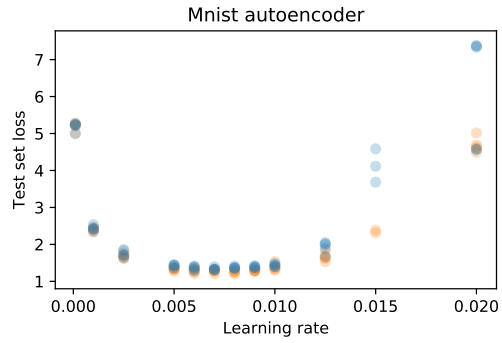
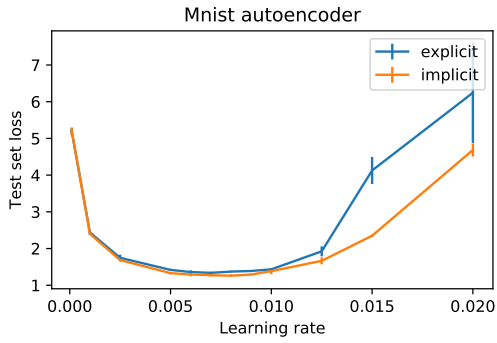
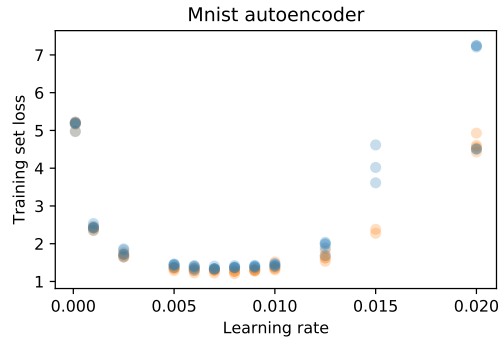
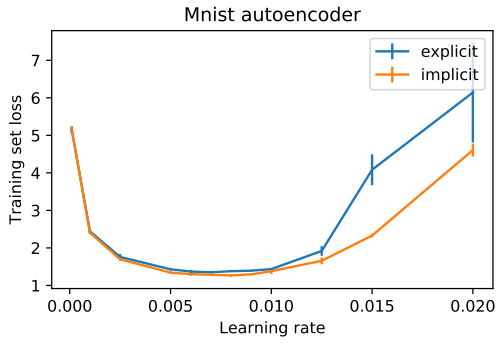


E.9 MNIST classification

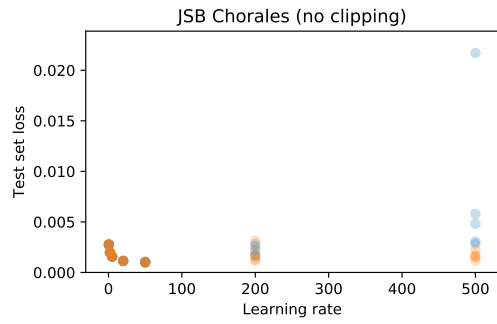
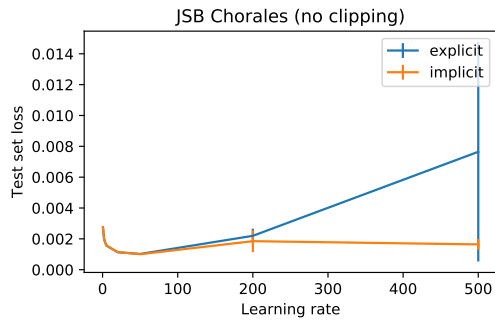
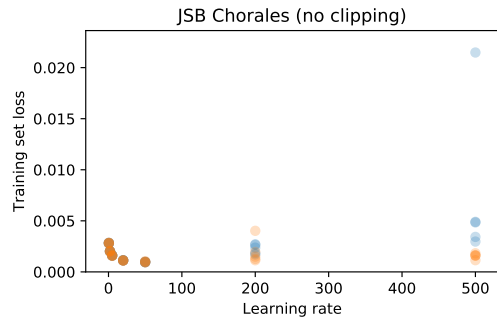
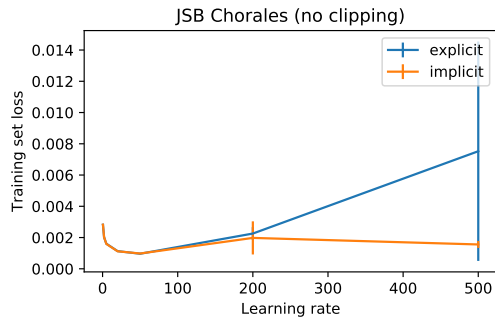


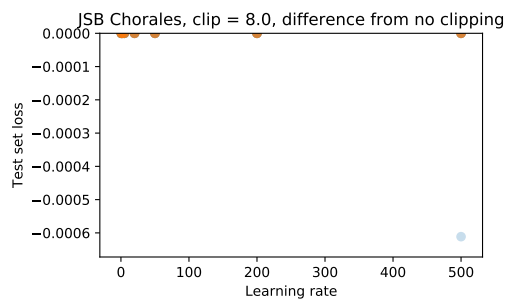
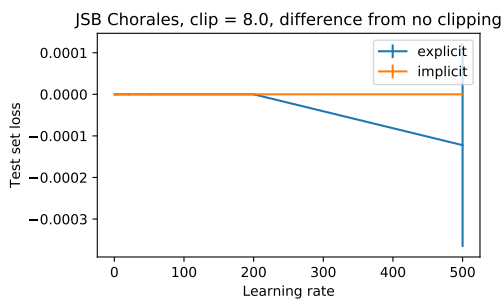
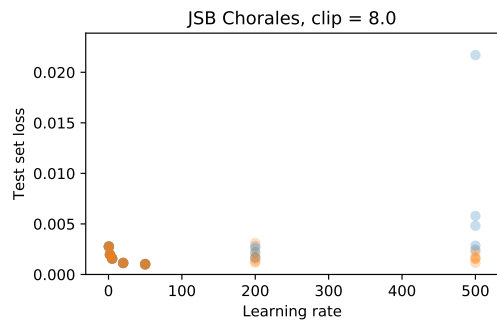
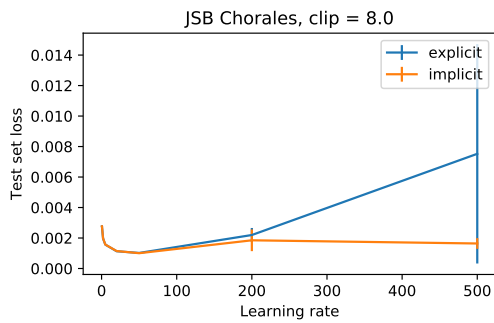
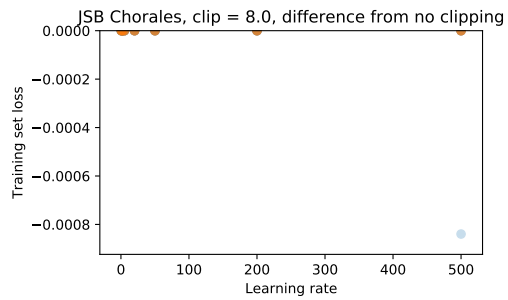
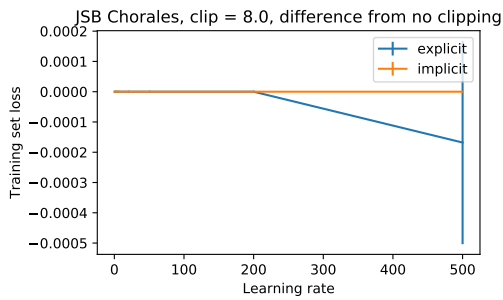
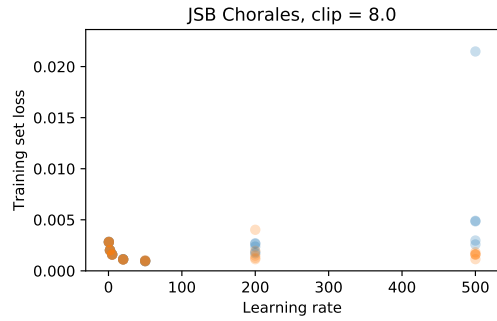
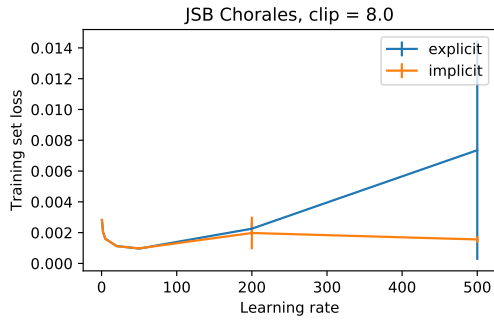


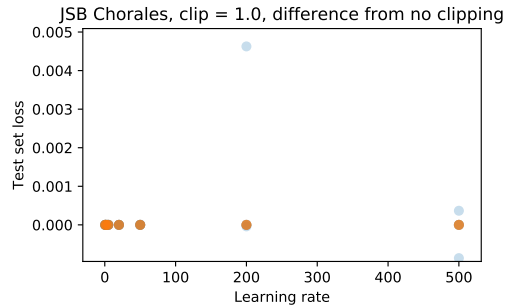
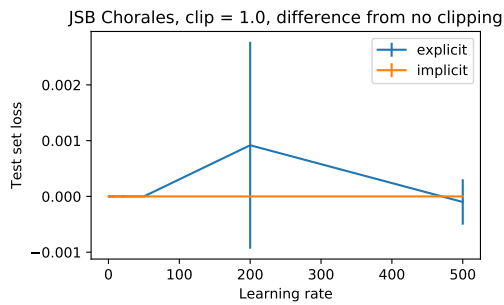
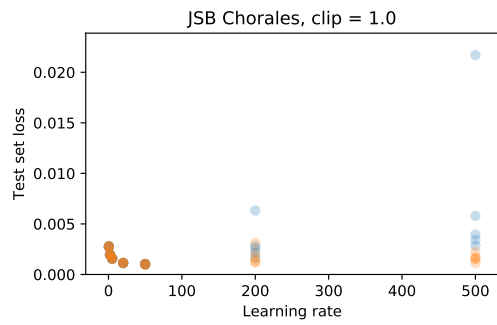
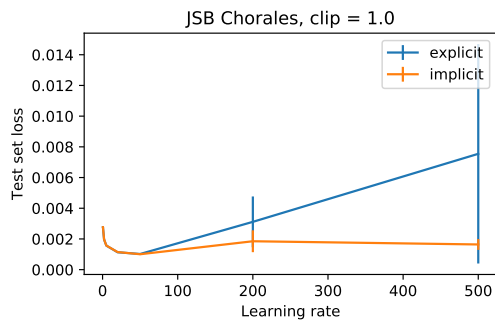
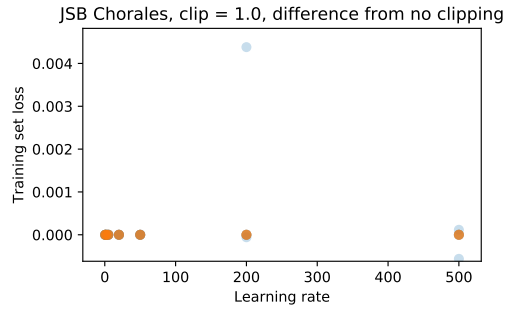
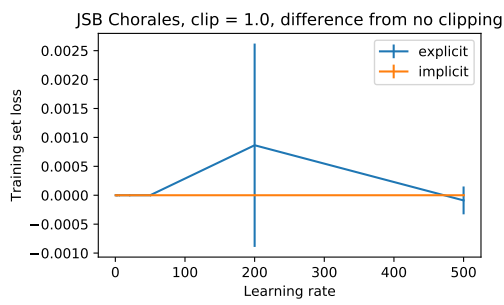
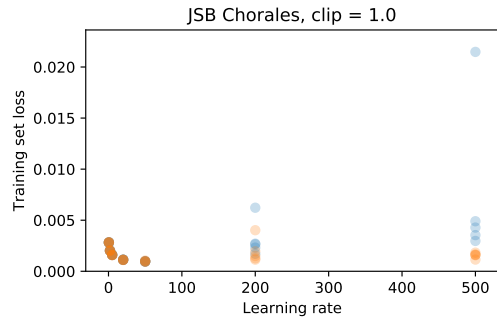
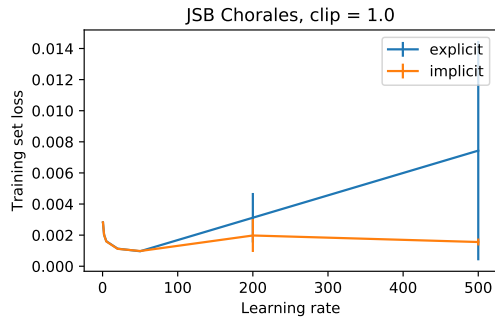
E.10 MNIST autoencoder

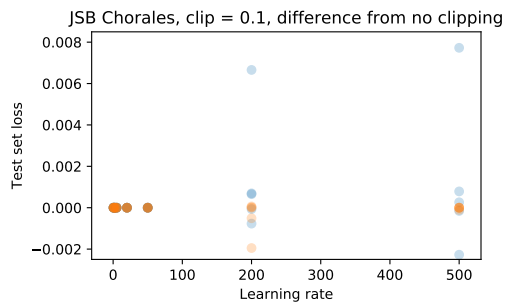
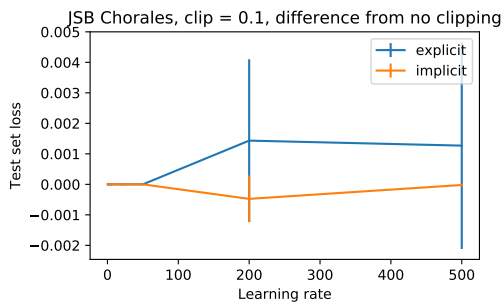
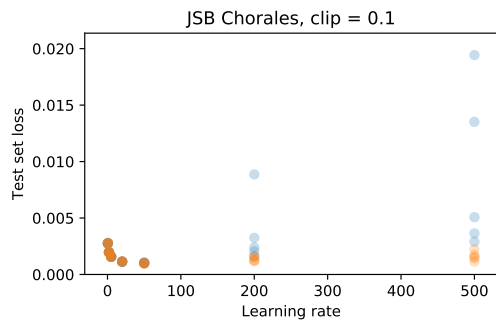
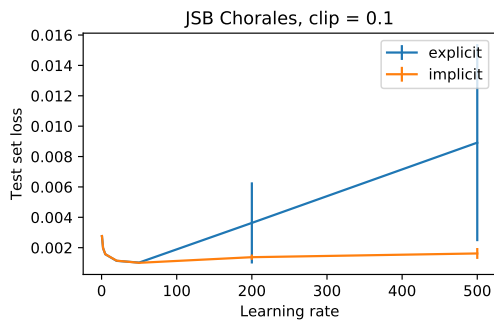
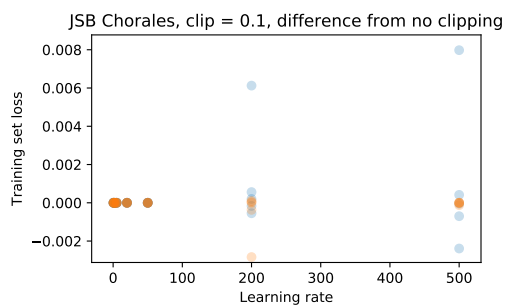
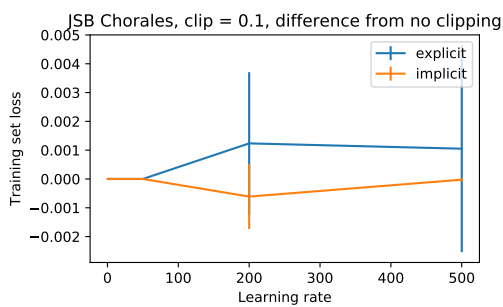
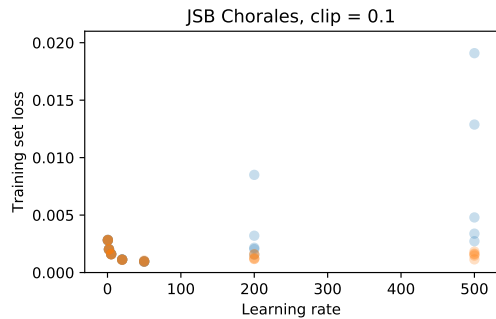
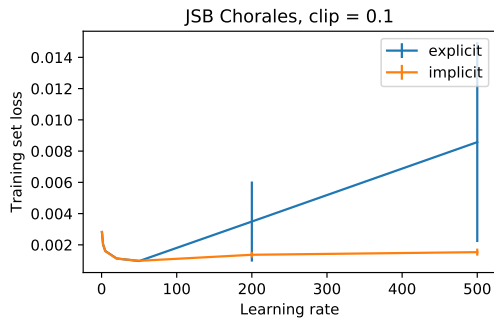


E.11 JSB Chorales

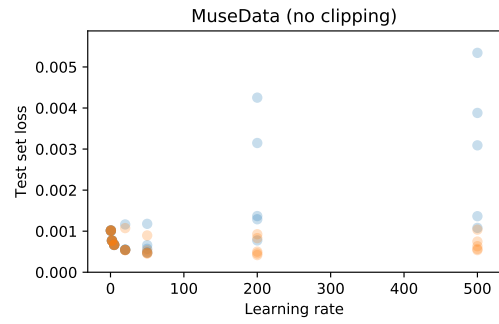
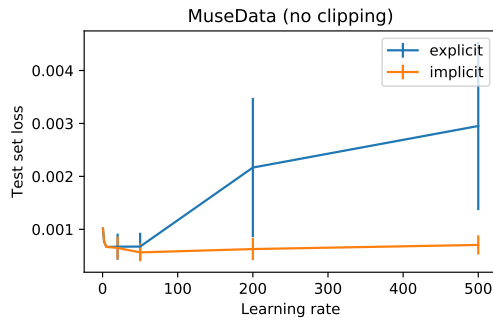
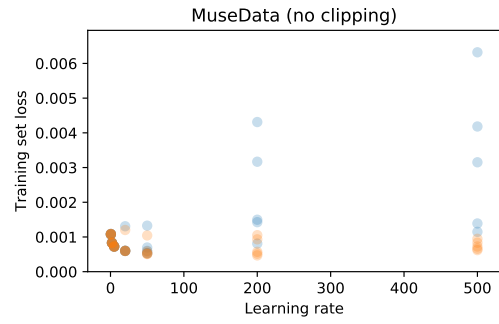
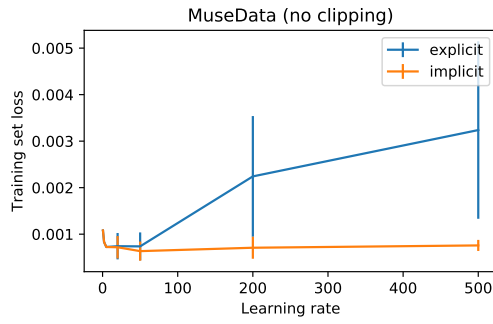


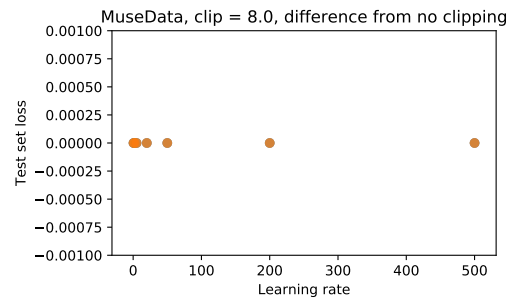
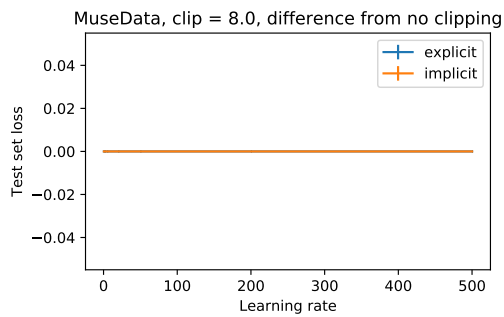
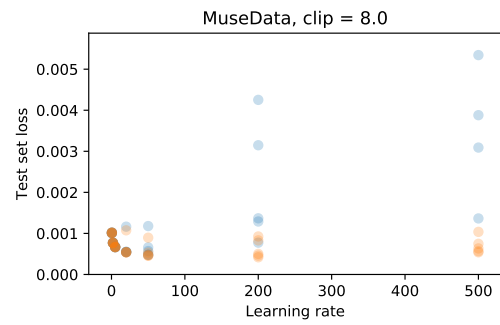
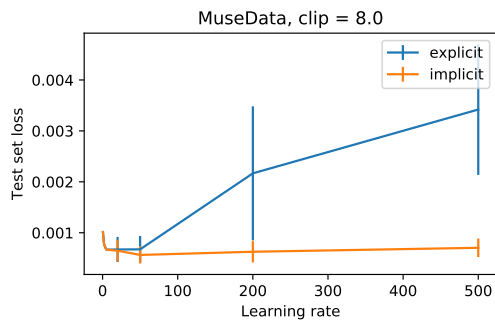
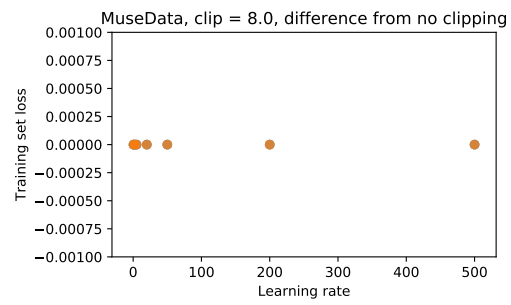
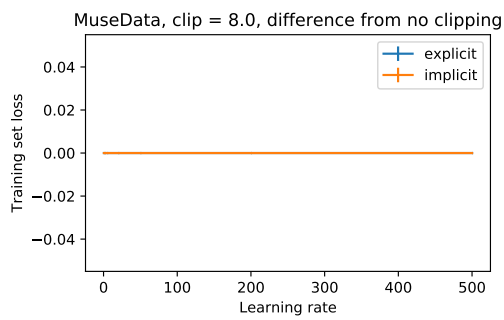
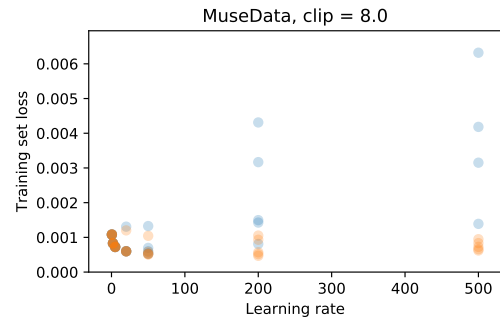
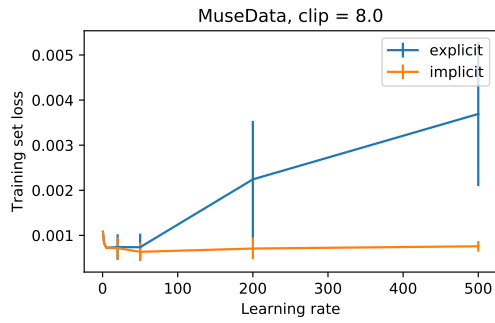




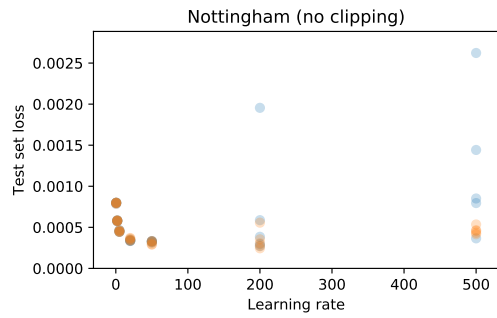
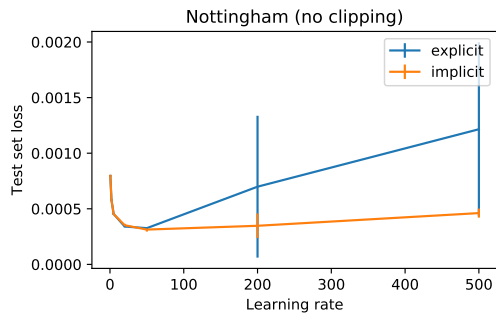
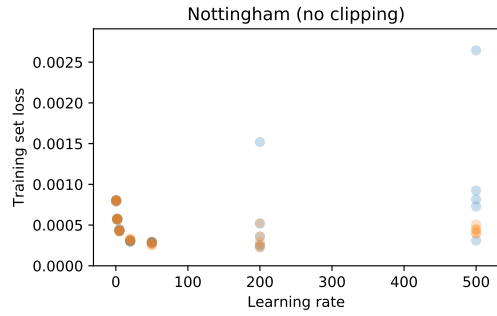
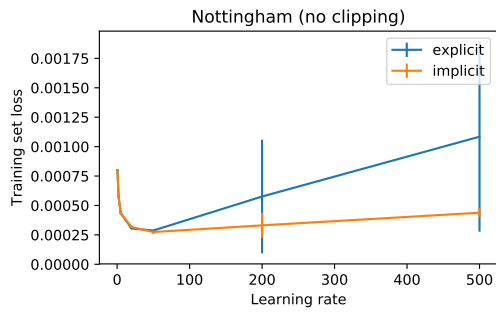


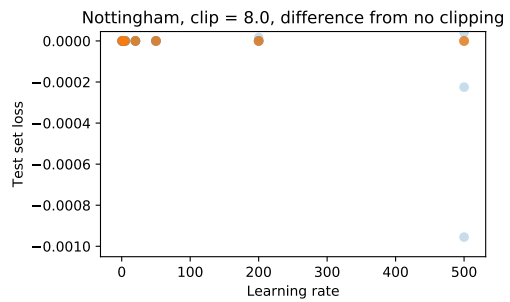
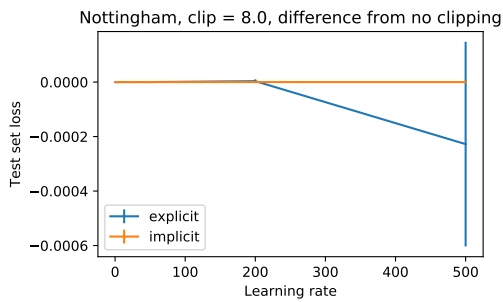
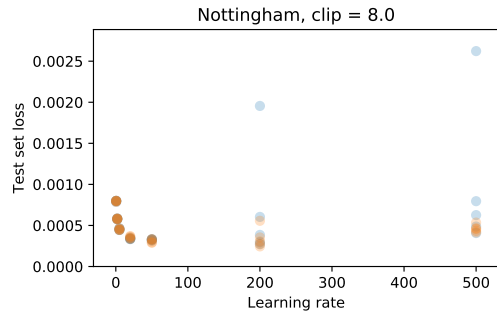
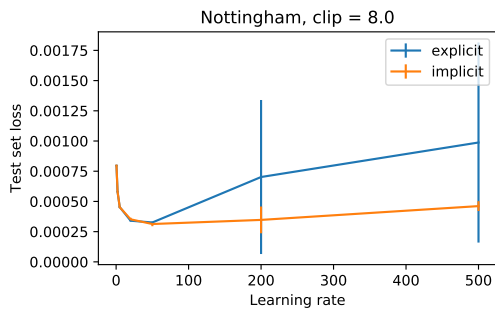
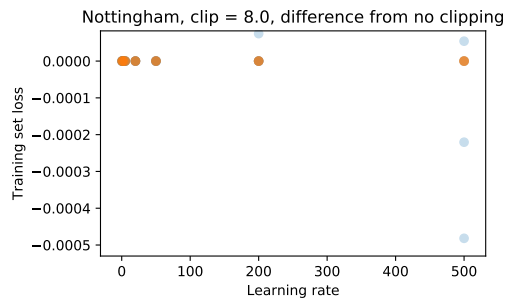
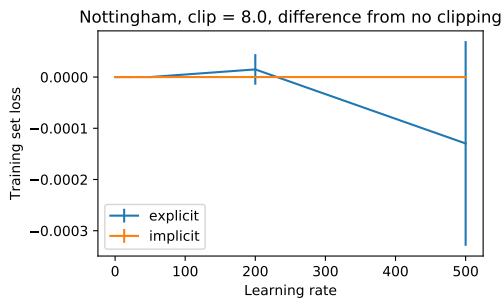
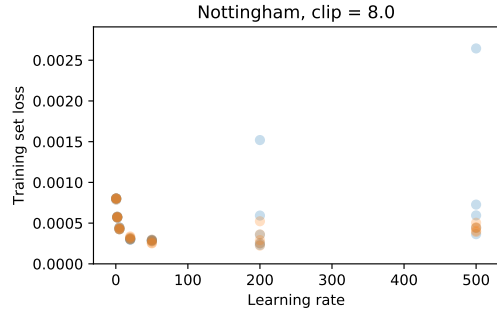
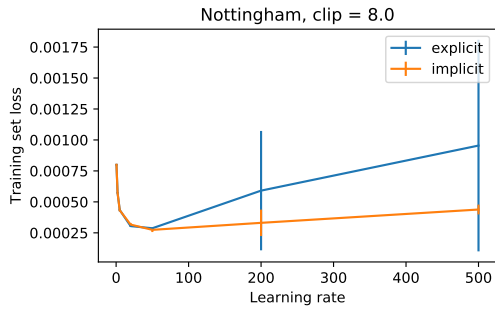
E.12 MuseData



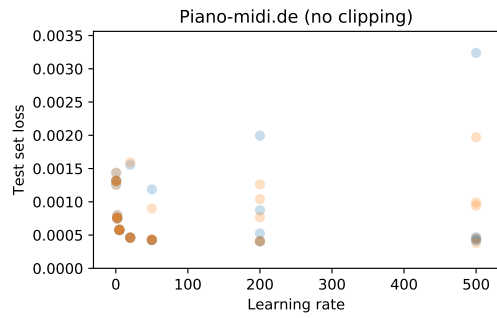
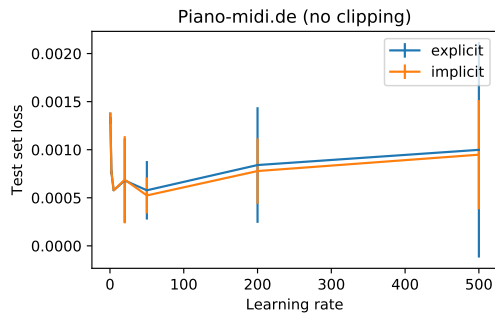
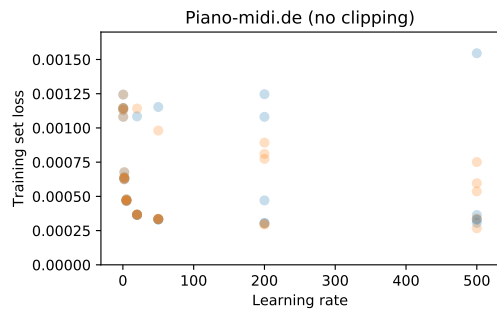
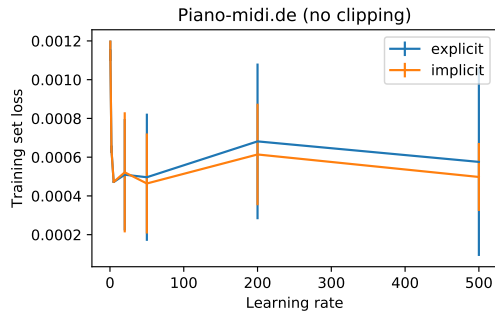


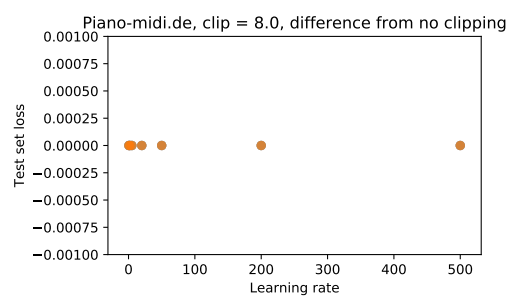
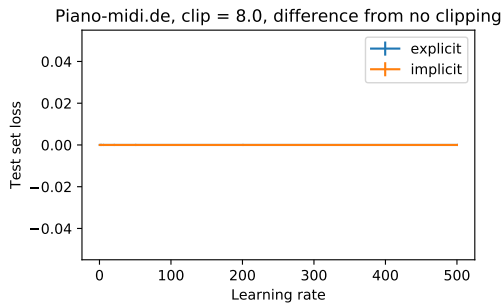
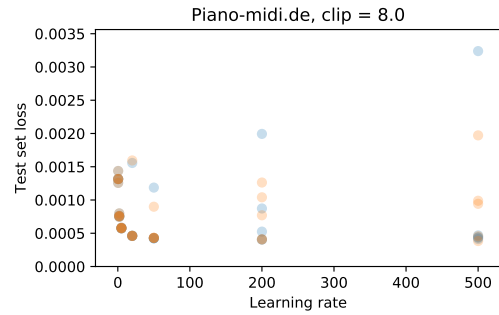
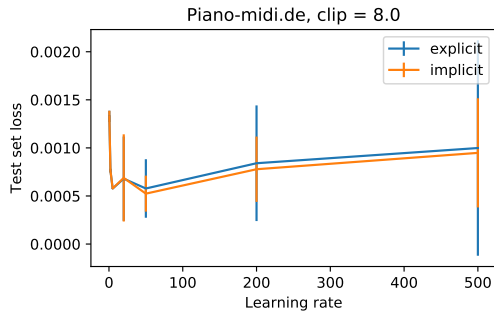
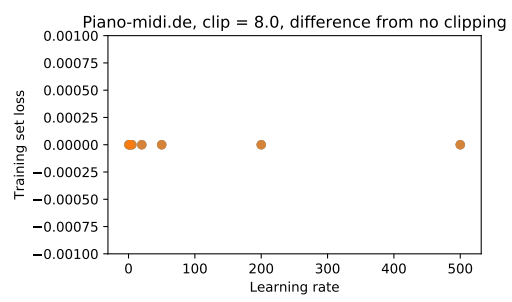
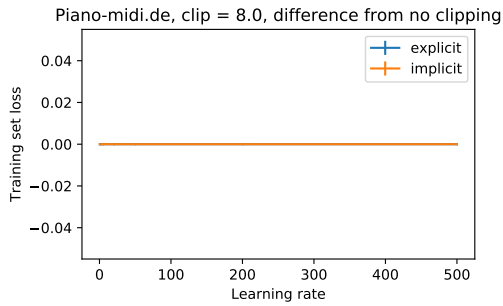
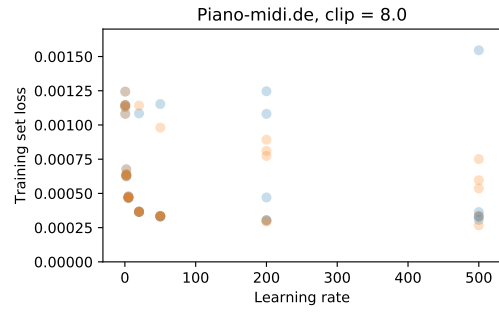
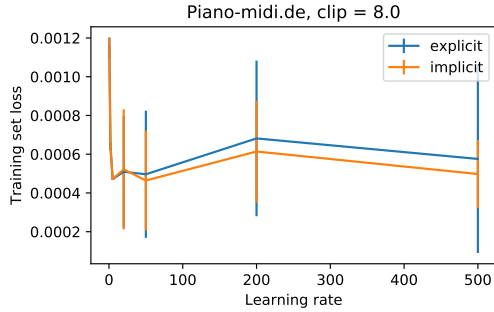
E.13 Nottingham

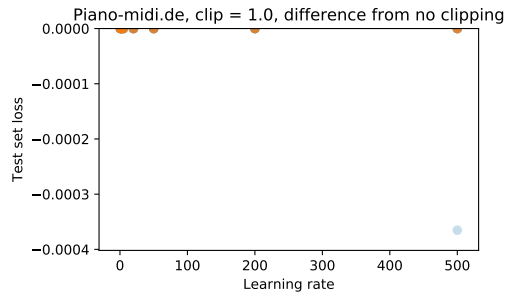
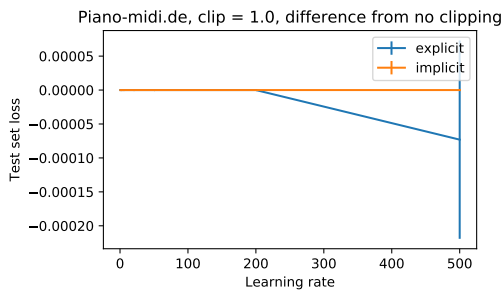
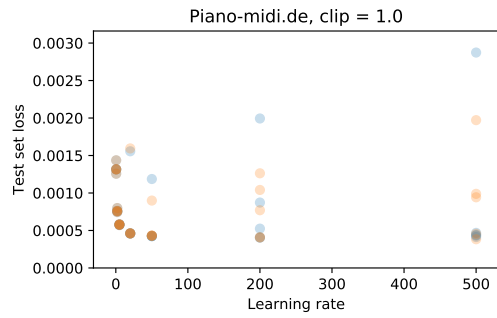
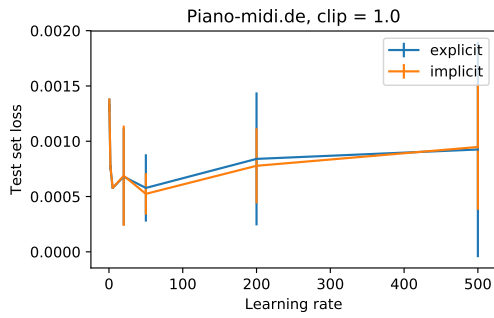
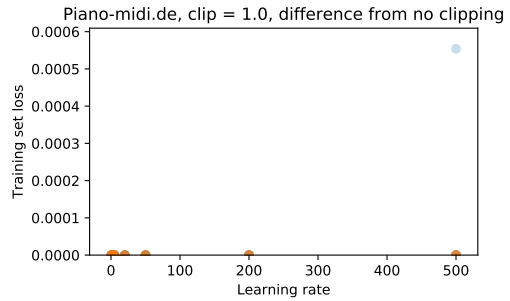
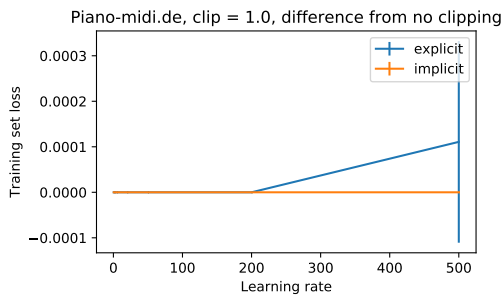
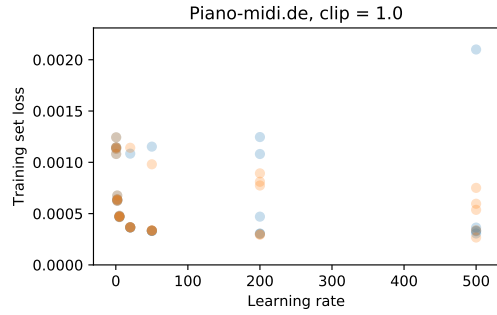
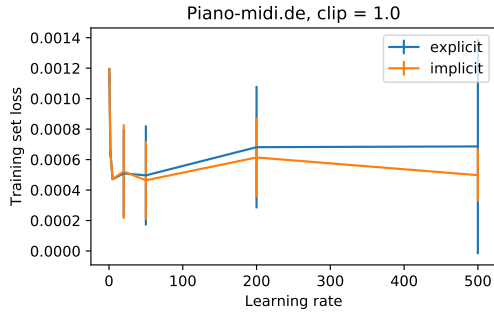


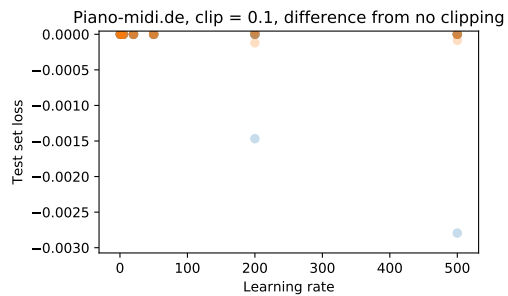
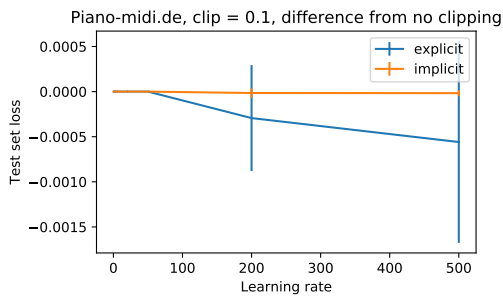
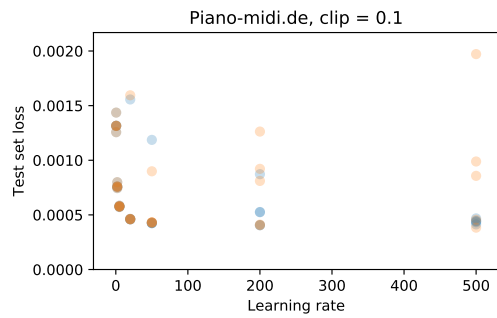
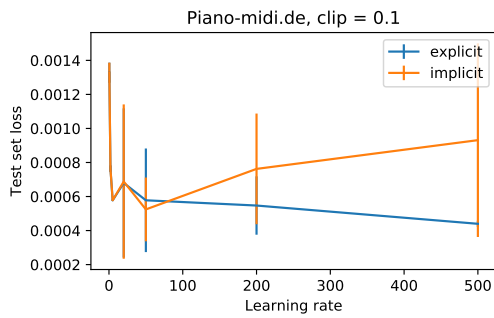
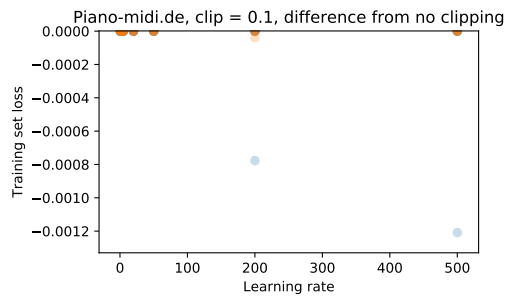
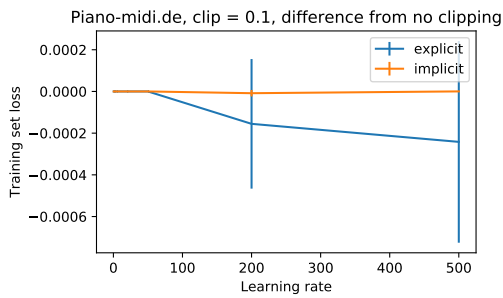
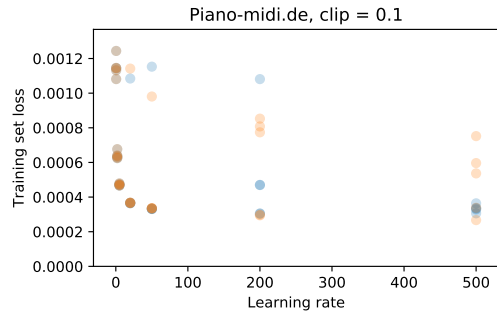
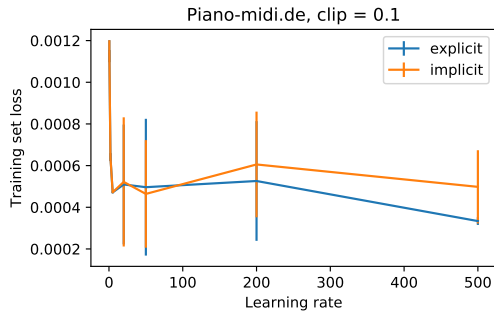


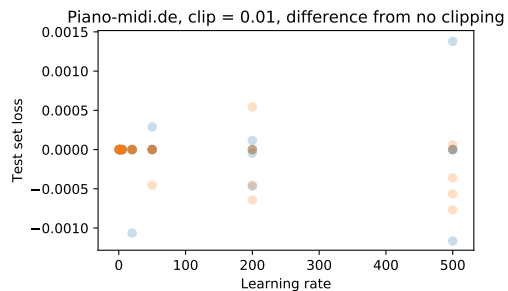
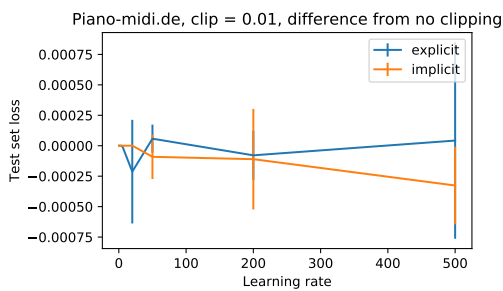
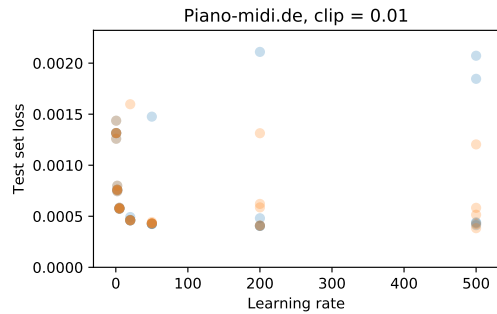
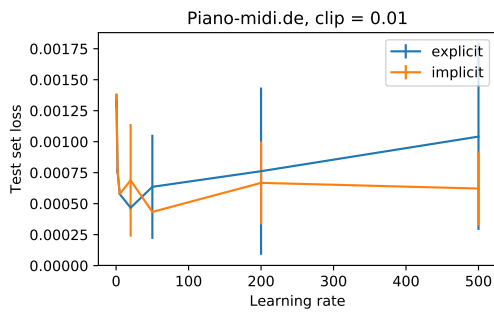
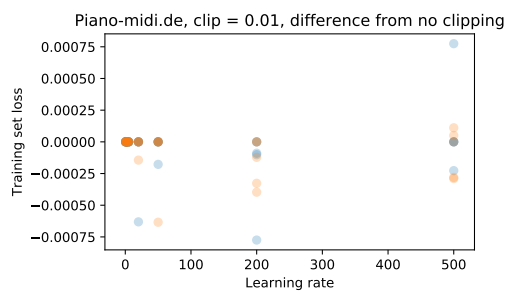
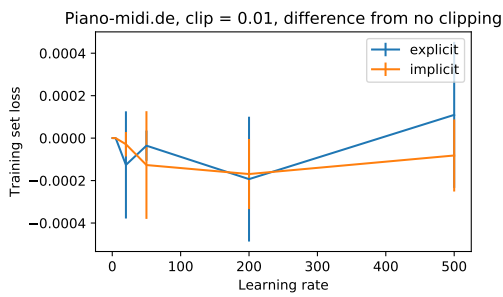
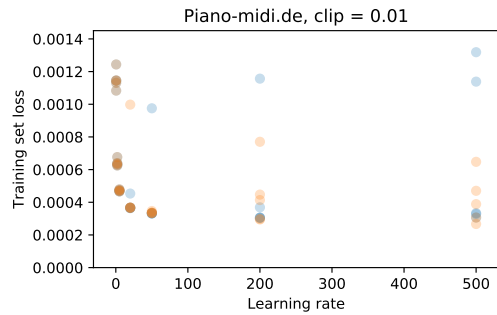
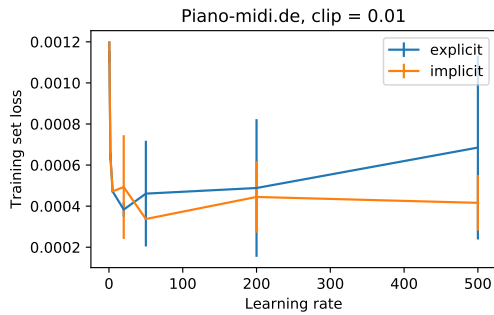
E.14 Piano-midi.de











E.15 UCI classification training losses

Here we display the training loss of IB and EB on each of the 121 UCI datasets at the end of the 10th epoch. We only ran each experiment with one random seed. The experiments are divided up into large (>1000 datapoints) and small (≤ 1000 datapoints).

The performance of EB and IB are very similar for the smaller learning rates. This is still the case at the optimal learning rate for each dataset. However, once either EB or IB moves one learning rate higher, the loss tends to explode. On average it is 892 times higher than the for the optimal loss. This is typical behavior for learning rate sensitivity, as is shown in [10, Fig 11.1, p. 425]. The fact that there is such a large explosion in the loss indicates that the learning rate grid is too coarse to pick up the differences in behaviors in learning rates slightly larger than the optimal learning rate. Hence it struggles to systematically distinguish between the performance of EB and IB.

Dataset (large)	Learning rate										SGD type
	0.001	0.01	0.1	0.5	1.0	3.0	5.0	10.0	30.0	50.0	
abalone	1.11	1.10	0.83	0.77	0.76	12.30	6.13	25.20	57.09	212.61	explicit
	1.11	1.10	0.83	0.77	0.77	2.65	3.18	22.95	98.31	84.63	implicit
adult	0.55	0.35	0.32	0.32	0.31	0.36	1.52	2.97	17.99	27.19	explicit
	0.55	0.35	0.32	0.32	0.32	0.34	1.15	4.31	12.22	20.27	implicit
bank	0.60	0.36	0.25	0.27	0.30	0.52	1.29	14.74	27.23	113.73	explicit
	0.60	0.36	0.25	0.27	0.29	0.35	1.46	21.44	65.24	19.08	implicit
car	1.18	1.01	0.85	0.50	0.39	0.59	5.28	4.55	53.97	106.93	explicit
	1.18	1.01	0.85	0.50	0.47	2.40	2.12	10.38	213.52	122.84	implicit
cardiotocography-10clases	2.30	2.18	1.24	0.68	0.68	4.36	6.71	13.91	59.09	156.53	explicit
	2.30	2.18	1.24	0.69	0.68	5.01	21.19	12.75	119.45	113.76	implicit
cardiotocography-3clases	1.09	0.74	0.30	0.21	0.21	0.67	5.59	19.91	23.95	173.83	explicit
	1.09	0.74	0.30	0.21	0.21	3.26	6.42	25.49	17.43	156.47	implicit
chess-krvk	2.81	2.45	1.96	1.70	1.75	2.13	2.22	10.26	39.35	144.99	explicit
	2.81	2.45	1.97	1.72	1.75	1.94	3.92	72.35	55.65	136.72	implicit
chess-krvvp	0.69	0.68	0.08	0.04	0.02	1.38	0.77	12.53	156.29	467.88	explicit
	0.69	0.68	0.08	0.07	0.07	0.33	2.80	12.91	26.88	56.18	implicit
connect-4	0.56	0.54	0.48	0.40	0.38	2.36	4.59	9.25	34.85	59.43	explicit
	0.56	0.54	0.50	0.44	0.46	3.23	4.64	11.31	33.66	52.39	implicit
contrac	1.08	1.07	1.07	0.99	0.96	1.00	5.34	17.32	149.70	133.28	explicit
	1.08	1.07	1.07	0.99	0.96	0.99	14.08	11.72	60.05	181.86	implicit
hill-valley	0.70	0.69	0.69	0.69	0.69	84.43	38.06	943.16	3267.16	1005.30	explicit
	0.70	0.69	0.69	0.69	0.70	168.00	180.79	907.54	2014.49	90.33	implicit
image-segmentation	1.95	1.94	0.95	0.20	0.12	9.13	11.97	13.45	95.62	72.58	explicit
	1.95	1.94	0.95	0.22	0.15	2.77	2.10	13.21	277.97	131.41	implicit
led-display	2.32	2.32	2.30	1.73	1.25	1.63	4.25	7.59	109.59	209.45	explicit
	2.32	2.32	2.30	1.73	1.26	3.13	5.43	30.01	93.78	240.85	implicit
letter	3.27	3.21	1.31	0.61	0.64	0.83	2.47	5.98	35.33	60.50	explicit
	3.27	3.21	1.31	0.59	0.68	0.84	1.85	5.92	27.24	39.06	implicit
magic	0.65	0.53	0.47	0.41	0.41	0.46	3.59	24.93	40.47	57.64	explicit
	0.65	0.53	0.48	0.42	0.43	0.53	5.43	5.41	41.77	146.46	implicit
mini-boone	0.37	0.29	0.23	0.21	0.22	1.40	5.60	18.28	60.37	190.87	explicit
	0.37	0.29	0.22	0.22	0.22	1.12	2.71	3.39	20.09	32.84	implicit
molec-biol-splce	1.05	0.98	0.36	0.31	0.25	5.32	9.87	30.26	146.88	227.42	explicit
	1.05	0.98	0.36	0.34	0.33	27.64	8.85	29.27	149.89	188.89	implicit
mushroom	0.69	0.36	0.01	0.00	0.00	0.00	0.06	1.96	157.31	87.08	explicit
	0.69	0.36	0.01	0.00	0.00	0.00	0.05	4.86	11.92	42.45	implicit
musk-2	0.49	0.19	0.08	0.03	2.75	34.14	112.76	228.01	436.03	288.58	explicit
	0.49	0.19	0.08	0.03	2.46	63.96	109.08	36.49	263.51	105.52	implicit
nursery	1.47	1.21	0.51	0.12	0.14	0.31	0.87	6.99	63.94	195.34	explicit
	1.47	1.21	0.52	0.18	0.12	0.19	1.36	33.21	129.24	514.70	implicit
oocytes-merluccius-nucleus-4d	0.65	0.63	0.61	0.69	0.73	18.79	19.89	82.75	767.96	917.21	explicit
	0.65	0.63	0.61	0.68	0.72	30.91	91.02	108.44	291.86	181.39	implicit
oocytes-merluccius-states-2f	1.04	0.88	0.35	0.22	0.20	1.46	3.09	34.59	255.92	35.96	explicit
	1.04	0.88	0.35	0.22	0.21	3.73	7.49	42.19	53.97	86.39	implicit

Dataset (large)	Learning rate										SGD type
	0.001	0.01	0.1	0.5	1.0	3.0	5.0	10.0	30.0	50.0	
optical	2.27	1.55	0.10	0.02	0.01	0.23	1.59	10.73	51.20	121.22	explicit
	2.27	1.55	0.10	0.03	0.01	0.22	0.42	3.97	8.87	15.60	implicit
ozone	0.51	0.18	0.09	0.09	0.10	9.91	11.00	8.83	115.42	30.89	explicit
	0.51	0.18	0.09	0.09	0.10	2.46	2.67	57.39	13.99	79.68	implicit
page-blocks	1.30	0.47	0.25	0.16	0.13	0.13	1.36	6.97	7.46	23.52	explicit
	1.30	0.47	0.25	0.16	0.15	0.13	2.79	24.66	43.27	111.66	implicit
pendigits	2.30	2.22	0.28	0.07	0.06	0.10	0.95	4.35	20.55	66.20	explicit
	2.30	2.22	0.28	0.05	0.05	0.18	0.26	0.72	12.03	32.69	implicit
plant-margin	4.60	4.59	3.91	1.39	0.82	6.24	16.50	52.11	152.54	299.85	explicit
	4.60	4.59	3.91	1.39	0.86	21.08	28.08	46.19	117.16	208.09	implicit
plant-shape	4.60	4.58	3.95	3.00	2.89	23.00	42.98	79.10	293.86	496.63	explicit
	4.60	4.58	3.95	3.00	2.87	19.54	43.80	85.42	234.65	572.32	implicit
plant-texture	4.61	4.59	4.17	1.20	0.55	0.34	16.13	39.06	123.57	193.97	explicit
	4.61	4.59	4.17	1.20	0.57	0.84	11.28	17.27	68.12	208.77	implicit
ringnorm	0.69	0.69	0.46	0.19	0.24	3.51	4.33	11.12	33.76	68.65	explicit
	0.69	0.69	0.47	0.22	0.21	2.64	5.10	53.34	29.11	72.79	implicit
semeion	2.18	1.04	0.08	0.01	0.02	5.35	21.05	92.46	978.63	1565.21	explicit
	2.18	1.04	0.08	0.01	0.00	90.42	1.71	7.28	149.68	559.76	implicit
spambase	0.67	0.36	0.18	0.16	0.17	8.17	2.06	20.93	67.37	102.59	explicit
	0.67	0.36	0.18	0.16	0.17	9.62	3.12	11.46	80.37	161.66	implicit
statlog-german-credit	0.73	0.65	0.59	0.46	0.47	0.54	19.04	28.39	223.84	279.24	explicit
	0.73	0.65	0.59	0.46	0.47	0.55	12.99	32.00	36.53	281.25	implicit
statlog-image	1.95	1.94	0.98	0.20	0.13	2.63	10.29	16.16	104.27	86.13	explicit
	1.95	1.94	0.98	0.20	0.18	3.61	7.49	62.98	65.65	62.29	implicit
statlog-landsat	1.73	0.90	0.37	0.32	0.30	3.21	7.15	25.85	51.35	53.25	explicit
	1.73	0.90	0.37	0.33	0.33	5.02	8.10	6.22	34.73	126.06	implicit
statlog-shuttle	0.80	0.18	0.03	0.04	0.01	0.02	0.54	0.71	40.30	4.51	explicit
	0.80	0.18	0.03	0.02	0.02	0.02	0.12	0.26	7.60	13.13	implicit
steel-plates	1.91	1.80	1.22	0.72	0.69	3.44	14.42	12.85	99.23	87.18	explicit
	1.91	1.80	1.22	0.73	0.70	68.19	11.35	169.10	136.68	340.84	implicit
thyroid	0.68	0.30	0.13	0.07	0.06	0.06	1.37	3.02	8.48	52.41	explicit
	0.68	0.30	0.13	0.07	0.07	0.09	2.71	6.23	33.58	51.21	implicit
titanic	0.64	0.63	0.63	0.52	0.52	0.59	0.98	10.04	61.18	87.35	explicit
	0.64	0.63	0.63	0.52	0.53	0.61	4.44	14.18	81.66	58.33	implicit
twonorm	0.69	0.55	0.06	0.06	0.06	0.07	0.59	5.49	23.61	26.69	explicit
	0.69	0.55	0.06	0.06	0.07	0.08	2.58	3.33	4.87	21.40	implicit
wall-following	1.38	1.18	0.67	0.33	0.34	1.56	6.02	19.54	63.01	149.71	explicit
	1.38	1.18	0.68	0.34	0.32	3.83	5.84	11.73	33.44	367.02	implicit
waveform	1.09	0.89	0.28	0.28	0.29	1.43	5.87	16.95	43.49	37.55	explicit
	1.09	0.89	0.28	0.28	0.29	1.81	6.47	9.13	32.50	30.61	implicit
waveform-noise	1.09	0.82	0.29	0.33	0.29	10.64	21.44	41.78	107.99	249.30	explicit
	1.09	0.82	0.29	0.33	0.31	7.92	9.56	10.69	87.91	35.45	implicit
wine-quality-red	1.78	1.55	1.20	0.96	0.95	1.01	4.72	16.11	72.08	206.43	explicit
	1.78	1.55	1.20	0.97	0.96	0.99	7.27	24.77	71.79	183.35	implicit
wine-quality-white	1.96	1.42	1.18	1.12	1.14	1.36	5.40	28.62	95.23	209.29	explicit
	1.96	1.42	1.18	1.12	1.15	1.30	22.65	22.89	267.55	226.40	implicit
yeast	2.29	2.07	1.73	1.21	1.21	2.11	5.53	16.11	40.73	139.51	explicit
	2.29	2.07	1.73	1.21	1.29	2.06	18.38	30.82	100.81	318.28	implicit

Dataset (small)	Learning rate										SGD type
	0.001	0.01	0.1	0.5	1.0	3.0	5.0	10.0	30.0	50.0	
acute-inflammation	0.69	0.69	0.69	0.69	0.67	0.45	9.87	26.80	58.27	30.87	explicit
	0.69	0.69	0.69	0.69	0.67	0.45	28.65	19.13	11.30	7.00	implicit
acute-nephritis	0.68	0.68	0.66	0.65	0.64	0.02	12.88	0.73	7.07	28.32	explicit
	0.68	0.68	0.66	0.65	0.64	0.02	9.84	0.00	13.72	21.91	implicit
annealing	1.52	1.20	0.73	0.49	0.57	2.24	10.88	38.62	183.52	209.44	explicit
	1.52	1.20	0.73	0.55	0.58	12.99	18.48	21.23	180.15	250.37	implicit
arrhythmia	2.46	1.92	0.63	0.25	24.92	57.87	162.63	256.21	507.11	1280.03	explicit
	2.46	1.92	0.63	0.23	30.57	48.03	111.98	329.23	1401.02	2270.51	implicit
audiology-std	2.89	2.85	2.55	0.93	0.42	28.32	27.10	57.28	165.67	270.77	explicit
	2.89	2.85	2.55	0.93	0.42	49.83	75.19	136.42	247.31	433.71	implicit
balance-scale	1.13	1.07	0.92	0.91	0.91	0.32	2.48	7.48	75.97	111.11	explicit
	1.13	1.07	0.92	0.91	0.91	0.32	19.65	30.05	151.05	267.63	implicit
balloons	0.70	0.69	0.68	0.68	0.68	0.68	6.96	43.68	25.14	88.85	explicit
	0.70	0.69	0.68	0.68	0.68	0.68	19.71	17.06	33.36	256.16	implicit
blood	0.69	0.62	0.54	0.54	0.54	0.54	0.54	17.12	67.33	85.15	explicit
	0.69	0.62	0.54	0.54	0.54	0.54	0.54	28.88	49.44	143.05	implicit
breast-cancer	0.71	0.68	0.63	0.62	0.59	0.61	20.42	33.63	38.61	97.66	explicit
	0.71	0.68	0.63	0.62	0.59	0.61	9.89	48.75	21.05	177.86	implicit
breast-cancer-wisc	0.70	0.67	0.64	0.10	0.09	0.11	2.13	3.60	3.59	16.08	explicit
	0.70	0.67	0.64	0.10	0.09	0.11	3.99	2.78	36.46	43.01	implicit
breast-cancer-wisc-diag	0.71	0.67	0.11	0.05	0.05	2.33	1.64	3.06	51.97	1399.89	explicit
	0.71	0.67	0.11	0.05	0.05	6.14	6.91	15.54	44.17	95.69	implicit
breast-cancer-wisc-prog	0.69	0.65	0.53	0.45	0.37	0.53	125.74	28.90	97.62	72.58	explicit
	0.69	0.65	0.53	0.45	0.37	0.49	25.71	36.27	54.02	1589.74	implicit
breast-tissue	1.78	1.78	1.78	1.77	1.75	1.18	6.23	35.95	69.66	510.77	explicit
	1.78	1.78	1.78	1.77	1.75	1.18	6.97	28.55	38.37	179.07	implicit
congressional-voting	0.71	0.69	0.67	0.66	0.63	0.68	13.56	69.97	139.57	503.67	explicit
	0.71	0.69	0.67	0.66	0.63	0.68	39.21	52.27	166.97	265.89	implicit
conn-bench-sonar-mines-rocks	0.69	0.69	0.59	0.30	0.32	75.14	93.29	204.05	363.93	1474.36	explicit
	0.69	0.69	0.59	0.30	0.33	33.36	51.40	62.84	447.59	387.23	implicit
conn-bench-vowel-deterding	2.41	2.41	2.40	1.33	1.02	1.00	4.54	13.65	105.52	270.46	explicit
	2.41	2.41	2.40	1.33	1.05	1.20	10.81	30.59	244.61	175.47	implicit
credit-approval	0.69	0.69	0.67	0.33	0.33	16.51	7.90	30.36	46.97	58.09	explicit
	0.69	0.69	0.67	0.34	0.33	1.66	8.54	42.96	31.86	35.54	implicit
cylinder-bands	0.71	0.68	0.64	0.49	0.50	5.17	20.72	75.39	299.83	175.94	explicit
	0.71	0.68	0.64	0.50	0.52	31.31	71.16	57.63	68.50	386.99	implicit
dermatology	1.81	1.78	1.32	0.23	0.09	5.17	1.43	28.02	62.58	374.63	explicit
	1.81	1.78	1.32	0.23	0.08	4.62	17.01	26.38	53.13	170.26	implicit
echocardiogram	0.67	0.65	0.59	0.25	0.19	0.19	12.02	73.34	95.15	136.16	explicit
	0.67	0.65	0.59	0.25	0.19	0.21	11.35	9.94	80.01	34.53	implicit
ecoli	2.11	2.06	1.79	1.19	0.96	0.97	23.58	13.47	90.18	77.99	explicit
	2.11	2.06	1.79	1.19	0.96	1.02	9.14	38.29	107.86	64.26	implicit
energy-y1	1.15	1.10	1.01	0.43	0.43	5.66	9.66	16.76	63.23	115.98	explicit
	1.15	1.10	1.01	0.45	0.49	4.34	1.61	17.47	44.28	59.35	implicit
energy-y2	1.18	1.11	1.02	0.40	0.39	0.44	1.36	5.68	14.01	38.33	explicit
	1.18	1.11	1.02	0.41	0.47	0.94	1.09	8.01	12.52	48.55	implicit
fertility	0.72	0.69	0.48	0.35	0.35	0.35	0.35	6.90	34.50	131.21	explicit
	0.72	0.69	0.48	0.35	0.35	0.35	0.35	62.82	11.22	17.92	implicit
flags	2.09	2.07	1.92	1.62	1.40	3.40	57.37	38.55	70.61	328.58	explicit
	2.09	2.07	1.92	1.62	1.40	19.65	38.18	103.61	150.33	631.23	implicit
glass	1.76	1.74	1.60	1.50	1.50	1.57	39.15	41.59	255.73	224.50	explicit
	1.76	1.74	1.60	1.50	1.50	1.59	11.74	27.31	140.43	378.32	implicit
haberman-survival	0.62	0.60	0.58	0.58	0.58	0.59	2.22	9.43	59.62	151.06	explicit
	0.62	0.60	0.58	0.57	0.58	0.59	2.16	11.38	35.12	166.79	implicit
hayes-roth	1.14	1.12	1.04	1.02	1.02	1.02	7.22	10.04	104.41	229.25	explicit
	1.14	1.12	1.04	1.02	1.02	1.02	8.16	26.48	31.05	127.38	implicit
heart-cleveland	1.64	1.58	1.30	0.91	0.90	0.90	7.38	16.45	108.54	99.98	explicit
	1.64	1.58	1.30	0.91	0.90	0.91	12.00	18.19	143.55	81.04	implicit
heart-hungarian	0.66	0.66	0.66	0.31	0.30	0.39	20.01	39.19	49.91	151.12	explicit
	0.66	0.66	0.66	0.31	0.30	0.37	18.31	5.64	211.14	81.71	implicit
heart-switzerland	1.65	1.63	1.51	1.35	1.33	1.32	42.48	47.01	296.09	295.82	explicit
	1.65	1.63	1.51	1.35	1.33	1.32	32.38	135.06	444.06	270.40	implicit
heart-va	1.65	1.63	1.55	1.50	1.48	1.39	24.42	59.53	434.70	186.13	explicit
	1.65	1.63	1.55	1.50	1.48	1.38	48.08	62.68	171.65	209.72	implicit
hepatitis	0.72	0.68	0.53	0.39	0.24	0.32	21.86	29.30	37.44	118.80	explicit
	0.72	0.68	0.53	0.39	0.24	0.35	32.01	19.00	41.54	111.05	implicit
horse-colic	0.70	0.68	0.65	0.34	0.34	0.32	24.44	60.72	42.39	335.00	explicit
	0.70	0.68	0.65	0.34	0.34	0.33	8.99	118.06	347.70	60.39	implicit
ilpd-indian-liver	0.70	0.66	0.60	0.59	0.55	0.53	16.40	55.36	45.47	299.05	explicit
	0.70	0.66	0.60	0.59	0.55	0.57	11.63	85.04	125.33	158.17	implicit
ionosphere	0.70	0.68	0.61	0.20	0.20	6.67	49.14	21.57	101.66	233.83	explicit
	0.70	0.68	0.61	0.21	0.22	34.03	9.97	64.38	768.47	572.70	implicit
iris	1.11	1.11	1.10	1.09	1.09	0.90	7.90	14.65	14.59	257.50	explicit
	1.11	1.11	1.10	1.09	1.09	0.77	9.25	26.47	147.58	175.54	implicit
lenses	1.09	1.07	0.98	0.91	0.91	0.91	10.79	13.42	38.90	30.30	explicit
	1.09	1.07	0.98	0.91	0.91	0.91	9.38	16.82	39.64	214.31	implicit
libras	2.72	2.68	2.09	0.93	0.72	26.84	19.45	79.46	196.99	349.34	explicit
	2.72	2.68	2.09	0.94	0.76	28.88	85.69	101.16	474.27	1377.74	implicit

Dataset (small)	Learning rate										SGD type
	0.001	0.01	0.1	0.5	1.0	3.0	5.0	10.0	30.0	50.0	
low-res-spect	2.19	1.78	0.43	0.25	11.66	14.48	53.18	222.26	605.63	449.56	explicit
	2.19	1.78	0.43	0.26	16.57	46.29	109.37	82.74	94.69	259.85	implicit
lung-cancer	1.11	1.10	1.04	0.27	0.03	28.79	87.95	149.18	1071.40	298.13	explicit
	1.11	1.10	1.04	0.27	0.03	95.18	87.43	284.11	543.03	359.73	implicit
lymphography	1.39	1.33	1.00	0.49	0.33	13.29	15.73	5.16	112.88	181.66	explicit
	1.39	1.33	1.00	0.49	0.34	6.11	14.23	10.87	34.13	261.76	implicit
mammographic	0.71	0.70	0.69	0.44	0.42	0.46	12.34	4.14	145.04	36.88	explicit
	0.71	0.70	0.69	0.44	0.42	0.44	10.77	9.93	116.31	244.93	implicit
molec-biol-promoter	0.69	0.69	0.65	0.11	0.01	36.10	27.78	109.47	258.44	974.85	explicit
	0.69	0.69	0.65	0.11	0.01	97.50	201.21	551.19	642.16	863.06	implicit
monks-1	0.69	0.69	0.69	0.69	0.62	0.71	17.77	17.11	89.50	138.78	explicit
	0.69	0.69	0.69	0.69	0.62	0.71	15.65	14.64	52.53	179.91	implicit
monks-2	0.68	0.66	0.65	0.65	0.65	0.65	4.11	7.96	135.92	180.88	explicit
	0.68	0.66	0.65	0.65	0.65	0.65	11.61	6.54	25.41	200.93	implicit
monks-3	0.70	0.69	0.69	0.68	0.51	0.76	4.16	11.69	45.17	222.38	explicit
	0.70	0.69	0.69	0.68	0.51	0.76	4.11	63.57	268.51	85.94	implicit
musk-1	0.69	0.63	0.32	0.59	35.26	48.17	358.12	325.26	2522.81	5693.28	explicit
	0.69	0.63	0.32	0.27	26.13	83.83	373.71	1592.32	5190.91	8195.80	implicit
oocytes-trisopterus-nucleus-2f	0.69	0.68	0.65	0.53	0.50	16.61	24.44	108.62	133.12	854.10	explicit
	0.69	0.68	0.65	0.53	0.52	22.13	109.88	27.77	631.40	859.68	implicit
oocytes-trisopterus-states-5b	1.00	0.89	0.41	0.24	0.21	7.33	15.53	14.13	42.37	516.20	explicit
	1.00	0.89	0.41	0.24	0.21	49.55	19.40	24.82	154.19	116.00	implicit
parkinsons	0.67	0.65	0.55	0.33	0.31	2.05	3.80	24.16	51.71	52.80	explicit
	0.67	0.65	0.55	0.33	0.31	20.58	14.53	90.82	37.16	468.79	implicit
pima	0.66	0.66	0.66	0.64	0.51	0.53	8.14	27.66	112.66	79.41	explicit
	0.66	0.66	0.66	0.64	0.51	0.52	2.47	69.41	143.07	249.05	implicit
pittsburg-bridges-MATERIAL	1.19	1.15	0.90	0.77	0.77	0.74	5.41	33.57	193.72	360.10	explicit
	1.19	1.15	0.90	0.77	0.77	0.74	15.25	37.79	203.28	303.36	implicit
pittsburg-bridges-REL-L	1.19	1.17	1.06	1.00	1.00	0.97	7.93	33.08	87.76	122.83	explicit
	1.19	1.17	1.06	1.00	1.00	0.97	11.10	25.15	124.80	330.23	implicit
pittsburg-bridges-SPAN	1.05	1.05	1.04	1.03	1.03	0.93	14.34	36.34	172.06	135.45	explicit
	1.05	1.05	1.04	1.03	1.03	0.93	2.40	45.68	166.73	279.46	implicit
pittsburg-bridges-T-OR-D	0.83	0.78	0.47	0.35	0.35	0.35	0.35	5.05	27.71	124.39	explicit
	0.83	0.78	0.47	0.35	0.35	0.35	0.35	21.00	38.70	23.87	implicit
pittsburg-bridges-TYPE	2.00	1.98	1.80	1.59	1.58	1.56	2.51	77.31	186.86	290.00	explicit
	2.00	1.98	1.80	1.59	1.58	1.56	5.37	82.37	272.11	350.51	implicit
planning	0.62	0.61	0.58	0.58	0.58	0.59	34.64	19.23	30.94	453.85	explicit
	0.62	0.61	0.58	0.58	0.58	0.59	19.01	15.86	166.14	261.24	implicit
post-operative	1.21	1.17	0.94	0.71	0.69	0.68	25.50	73.03	60.28	83.88	explicit
	1.21	1.17	0.94	0.71	0.69	0.68	25.03	50.13	90.23	71.85	implicit
primary-tumor	2.70	2.68	2.50	2.15	1.83	13.21	17.81	41.57	99.73	94.32	explicit
	2.70	2.68	2.50	2.15	1.83	10.32	15.55	35.04	70.16	326.01	implicit
seeds	1.11	1.10	1.09	0.62	0.47	0.68	8.84	13.44	28.41	32.21	explicit
	1.11	1.10	1.09	0.62	0.47	7.20	5.44	28.78	87.84	85.50	implicit
soybean	2.90	2.86	2.43	0.65	0.21	2.12	5.69	33.16	151.98	119.04	explicit
	2.90	2.86	2.43	0.66	0.22	9.36	20.48	32.44	161.14	288.93	implicit
spect	0.70	0.69	0.67	0.44	0.45	0.57	54.69	105.29	263.16	159.21	explicit
	0.70	0.69	0.67	0.44	0.45	0.47	18.18	159.16	21.86	567.59	implicit
spectf	0.69	0.64	0.49	0.38	0.42	20.77	6.86	28.35	622.85	585.05	explicit
	0.69	0.64	0.49	0.37	0.51	80.29	132.31	27.83	130.49	1229.86	implicit
statlog-australian-credit	0.68	0.66	0.64	0.64	0.64	0.64	19.39	35.72	31.33	78.80	explicit
	0.68	0.66	0.64	0.64	0.64	0.64	73.71	98.74	228.37	448.01	implicit
statlog-heart	0.69	0.69	0.69	0.32	0.33	6.74	4.19	9.82	143.11	37.86	explicit
	0.69	0.69	0.69	0.32	0.33	15.30	0.98	28.84	157.01	541.23	implicit
statlog-vehicle	1.39	1.39	1.31	0.90	0.78	16.15	9.25	42.65	163.61	403.98	explicit
	1.39	1.39	1.31	0.89	0.70	32.42	20.88	93.00	74.45	656.19	implicit
synthetic-control	1.80	1.72	0.70	0.06	5.96	24.28	43.88	113.24	69.17	482.32	explicit
	1.80	1.72	0.70	0.06	9.76	24.30	50.20	110.53	164.13	692.48	implicit
teaching	1.11	1.11	1.09	1.09	1.09	1.11	16.23	47.19	43.59	92.10	explicit
	1.11	1.11	1.09	1.09	1.09	1.11	12.49	21.53	266.23	199.40	implicit
tic-tac-toe	0.68	0.66	0.64	0.52	0.10	2.05	4.13	45.16	156.90	81.64	explicit
	0.68	0.66	0.64	0.52	0.09	10.22	40.48	53.51	47.37	200.14	implicit
trains	0.70	0.70	0.67	0.04	0.01	0.00	16.94	8.70	153.88	503.41	explicit
	0.70	0.70	0.67	0.04	0.01	0.00	55.28	83.36	0.00	0.00	implicit
vertebral-column-2clases	0.68	0.66	0.63	0.58	0.37	6.00	13.78	9.92	23.02	189.26	explicit
	0.68	0.66	0.63	0.58	0.37	0.39	3.75	13.45	106.58	52.45	implicit
vertebral-column-3clases	1.10	1.09	1.05	0.77	0.54	7.37	17.75	12.02	44.07	81.04	explicit
	1.10	1.09	1.05	0.77	0.53	2.55	9.28	7.79	42.32	40.59	implicit
wine	1.12	1.12	1.09	0.53	0.46	5.43	3.44	9.22	43.31	62.74	explicit
	1.12	1.12	1.09	0.53	0.47	5.78	37.86	96.27	64.82	88.60	implicit
zoo	1.92	1.91	1.83	1.57	1.01	6.70	6.23	33.11	172.96	380.68	explicit
	1.92	1.91	1.83	1.57	1.01	6.58	22.16	56.49	198.40	189.51	implicit